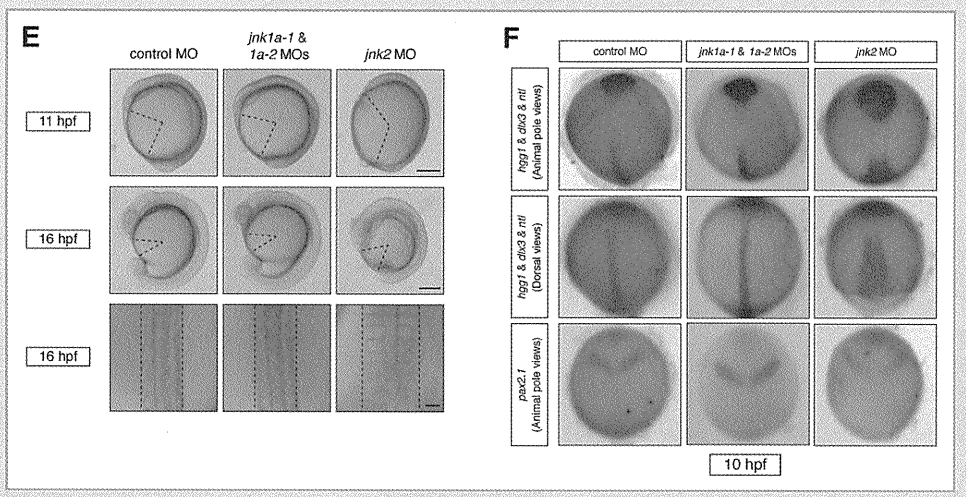

Fig. 3. Jnk2 is required for proper CE movements in zebrafish. A: Jnk is activated by *wnt11* or *wnt5* overexpression. Pooled extracts of 25 embryos overexpressing *wnt11* were analyzed by Western blotting (top). Levels of phospho-Jnk (p-Jnk) were increased compared to the control but total Jnk (55 and 46 kDa isoforms) was unchanged. Pooled extracts of 25 embryos overexpressing *wnt5* were analyzed by Western blotting (bottom). Gapdh, internal control. B: Markedly reduced Jnk phosphorylation in *mkk4b* morphants. Twenty-five embryos injected with 0.4 pmol of *mkk4a* MO, *mkk4b* MO, or *mkk7* MO were analyzed at the shield stage by Western blotting to detect Jnk and p-Jnk. C: Validation of *jnk1a* MOs. Schematic illustrations of the target sites of the *jnk1a-1* MO and *jnk1a-2* MO are shown in the top and center panels, respectively. Arrows represent the primer pairs used in the RT-PCR evaluation of MO efficacy. The bottom panel shows an RT-PCR analysis of the effects of these MOs on *jnk1a-1* and *jnk1a-2* expression. Total RNA was extracted at 8 hpf from untreated WT embryos, or WT embryos co-injected with *jnk1a-1* MO and *jnk1a-2* MO (0.8 pmol each). *Jnk1a-1* MO and *jnk1a-2* MO prevent correct splicing of *jnk1a-1* and *jnk1a-2* pre-mRNAs, respectively, resulting in a reading-frame shift and production of mutant proteins. D: Validation of *jnk2* MO. Top panel depicts the location of the target site of *jnk2* MO and the primer pairs used for RT-PCR. The bottom panel shows an RT-PCR analysis of the effect of *jnk2* MO. Total RNA was extracted from WT embryos injected with control MO (0.8 pmol) or *jnk2* MO (0.7 pmol). *Jnk2* MO induces defective splicing. E: Gross appearance of *jnk* morphants. Images of live embryos injected with control MO (0.8 pmol), *jnk1a-1* MO plus *jnk1a-2* MO (0.8 pmol each), or *jnk2* MO (0.7 pmol) were acquired at 11 and 16 hpf. These embryos are viewed laterally, with anterior to the top. *Jnk1* MOs cause no gross morphological defects, whereas *jnk2* morphants exhibit a shortening of body length. At 16 hpf, the notochord and somites are wider in the *jnk2* morphant than in the control (dorsal view). Scale bars = 200 μm (row 1); 200 μm (row 2); 50 μm (row 3). F: Impaired CE in *jnk2* morphants. *Jnk* morphants and controls were analyzed by whole-mount in situ hybridization for the expression of tissue-specific genes at the tailbud stage (10 hpf). *Jnk1a* morphants showed normal marker expression. In *jnk2* morphants, the position of the prechordal plate (*hgg1*) is more posterior and broader than in the control. Expression of *dlx3* (neuroectoderm) reveals a broader neural plate, and the notochord (*ntl*) is shorter and broader. The midbrain/hindbrain boundary (*pax2.1*) has expanded laterally.

of body length at 11, 16, and 24 hpf and exhibited broader notochords and somites at 16 hpf (Fig. 5A), reminiscent of the *mkk4b* morphant phenotype (Fig. 2B). With respect to marker expression patterns, the expression of the organizer marker *gsc* was not changed in *wnt11*-overexpressing embryos compared to control embryos injected with *egfp* mRNA (Fig. 5B, top). At the tailbud stage, *wnt11*-overexpressing embryos showed a more posteriorly positioned prechordal plate (*hgg1*), a wider neural plate (*dlx3*), a shorter and broader notochord (*ntl*), and a laterally expanded midbrain/hindbrain boundary (*pax2.1*) than did controls (Fig. 5B, bottom). These observations imply that the level of *wnt11* mRNA present critically influences CE.

MKK4B MORPHANTS SHOW INCREASED *WNT11* EXPRESSION IN THE ORGANIZER AND MARGIN REGIONS

We next used whole-mount in situ hybridization to localize the increased *wnt11* expression in Mkk4b-depleted embryos. During gastrulation in control MO-injected embryos, *wnt11* expression became prominent in the lateral and ventral germ ring (margin region) but was downregulated within the region of shield formation (i.e., the organizer) (Fig. 6A; 6 hpf). *Wnt11* expression near the margin persisted throughout gastrulation, although the staining intensity gradually decreased in the ventral region. *Wnt11* expression remained high in the dorsal region, which converges with the tailbud (Fig. 6A; 8 and 10 hpf). In contrast, during gastrulation in *mkk4b* morphants, *wnt11* expression was significantly increased in both the organizer and margin regions (Fig. 6A; 6 hpf). By late gastrulation, *wnt11* expression was strongly upregulated in all domains (Fig. 6A; 8 and 10 hpf). On the other hand, the expression pattern of *wnt5* in *mkk4b* morphants matched that of controls (Fig. 6B).

IMPAIRED MKK4B FUNCTION PROMOTES *WNT11* TRANSACTIVATION IN A NON-CELL-AUTONOMOUS MANNER

To determine whether *wnt11* was a direct transcriptional target of Mkk4b-Jnk signaling, we generated small clones of *mkk4b*-deficient zebrafish cells within whole embryos by co-injecting *mkk4b* MO together with *egfp* mRNA into one blastomere of a 32- or 64-cell embryo (Fig. 7A). We subsequently examined the location of the EGFP-labeled descendant cells at the shield stage (Fig. 7B, top row) and analyzed *wnt11* expression pattern by whole-mount in situ hybridization (Fig. 7B, bottom row). *Wnt11* expression was significantly elevated even in the embryonic region that did not overlap with the lineage label marking the progeny of *mkk4b* MO-

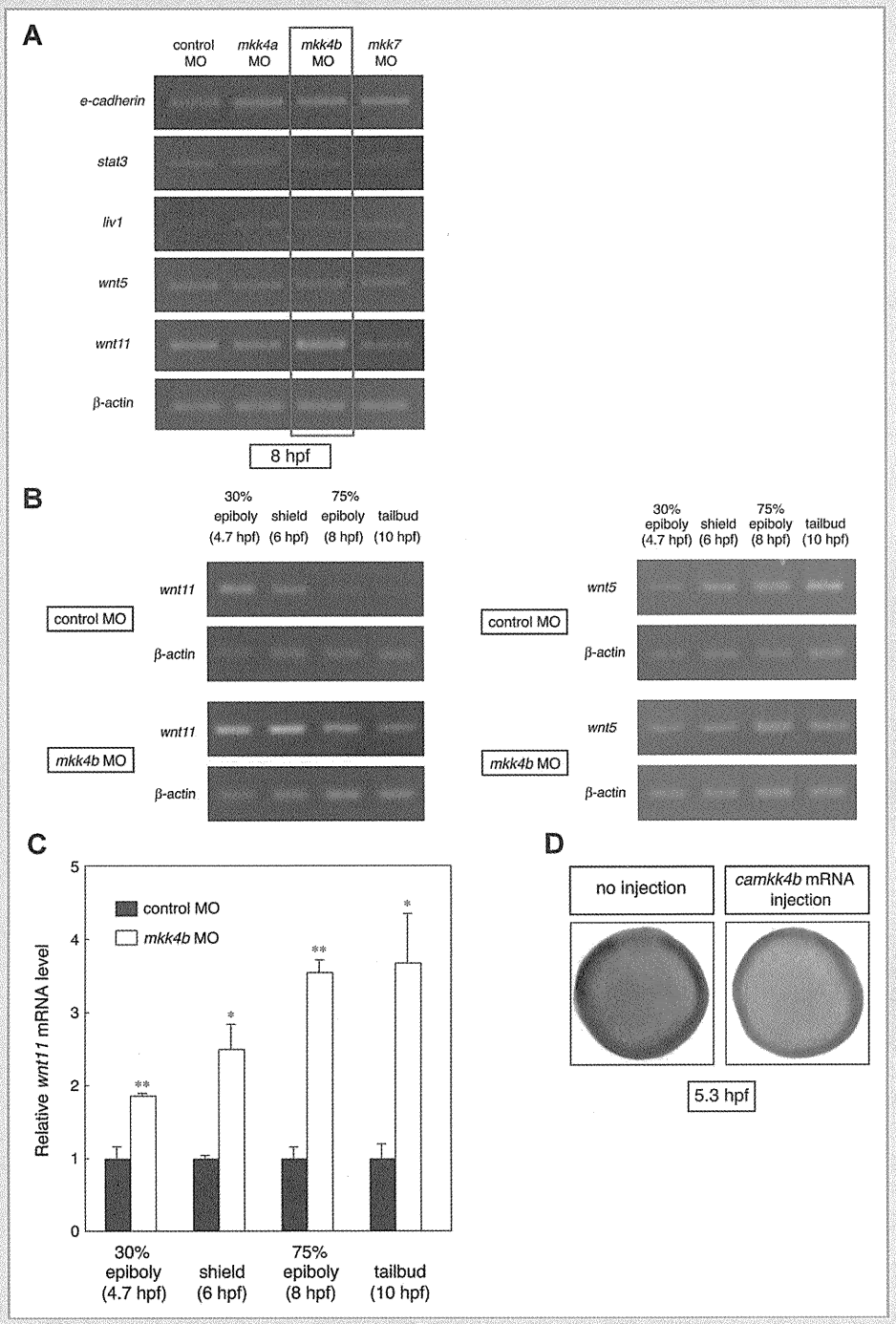

Fig. 4. Identification of *wnt11* as a downstream component of Mkk4b–Jnk signaling in the non-canonical Wnt pathway. A: Specific upregulation of *wnt11* in *mkk4b* morphants. Total RNA was isolated from control, *mkk4a*, *mkk4b*, and *mkk7* morphants at the 75% epiboly stage (8 hpf) and subjected to RT-PCR to detect expression of the indicated mRNAs. *β-Actin*, internal control. B: Upregulation of *wnt11* but not *wnt5* in *mkk4b* morphants throughout early embryogenesis. Total RNA was isolated from control and *mkk4b* morphants at the indicated stages and subjected to RT-PCR to detect expression of *wnt11* (left) and *wnt5* (right) mRNAs. C: Quantitative RT-PCR analysis of *wnt11* mRNA expression in *mkk4b* morphants. For all quantitative PCR experiments, *wnt11* cDNA amplification was standardized to the amplification of *β-actin* cDNA. *Wnt11* expression in *mkk4b* morphants was normalized to that in controls (assigned an arbitrary value of 1). Data shown are the mean ± SEM of three independent experiments ($^{*}P < 0.05$; $^{**}P < 0.01$ vs. control). D: Mkk4b–Jnk signaling represses *wnt11* expression. WT embryos were left untreated or injected with *camkk4b* mRNA (40 pg) and subjected to whole-mount in situ hybridization to detect *wnt11* at the 50% epiboly stage (5.3 hpf; animal pole views). Decreased *wnt11* expression was observed in *camkk4b*-overexpressing embryos (right) compared with uninjected embryos (left).

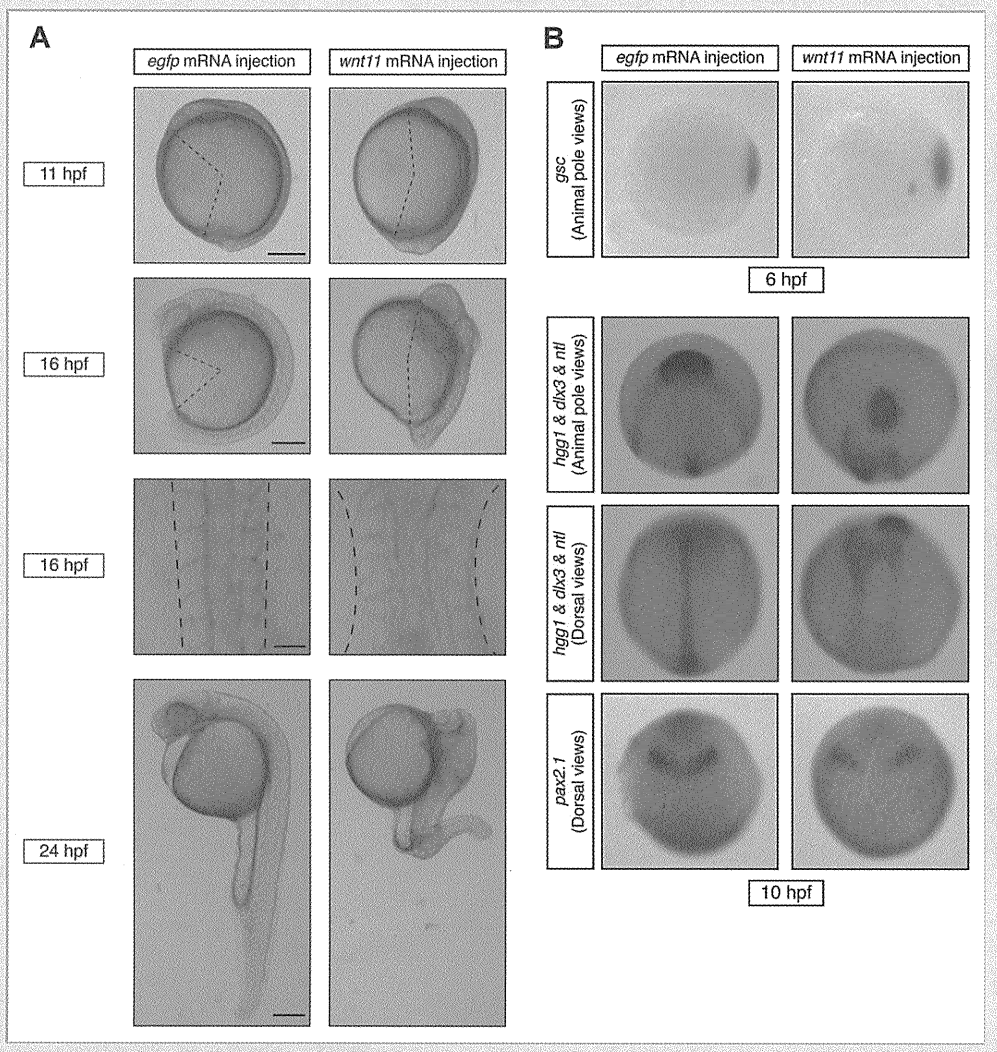

Fig. 5. Overexpression of *wnt11* induces CE abnormalities. A: Altered gross appearance. WT embryos were injected with either *egfp* mRNA (100 pg; control) or *wnt11* mRNA (75 pg), and the gross phenotype of the embryos was examined at 11, 16, and 24 hpf (rows 1, 2, and 4, respectively). These embryos are viewed laterally, with the anterior to the top. A shortening of body length can be seen as early as 11 hpf in the *wnt11*-overexpressing embryos. Row 3 shows that the notochord and somites are wider in the *wnt11*-overexpressing embryos than in the controls at 16 hpf (dorsal view). Scale bars = 200 μm (row 1); 200 μm (row 2); 50 μm (row 3); 200 μm (row 4). B: Impaired CE in *wnt11*-overexpressing embryos. WT embryos were injected with *egfp* or *wnt11* mRNA (100 pg), and analyzed by whole-mount in situ hybridization for the expression of tissue-specific genes at the shield stage (6 hpf) and the tailbud stage (10 hpf). The expression pattern of the organizer marker *gsc* is similar in the *wnt11*-overexpressing embryos and controls. However, the position of the prechordal plate (*hgg1*) is more posterior in *wnt11*-overexpressing embryos compared to the control. Expression of *dlx3* (neuroectoderm) reveals a broader neural plate, and the notochord (*ntl*) is shorter and broader. The midbrain/hindbrain boundary (*pax2.1*) has expanded laterally.

injected cells (Fig. 7B). Thus, activation of the Mkk4b–Jnk signaling pathway in zebrafish embryos represses *wnt11* expression in a non-cell-autonomous fashion.

Taken together, our findings suggest that the suppression of *wnt11* transcription by Jnk activation is important for the precise regulation of vertebrate CE, and establish a model in which non-canonical Wnt signaling leading to Jnk activation represses expression of the CE-triggering ligand Wnt11 (Fig. S7).

DISCUSSION

In this study, we examined the role of Jnk signaling during the early embryogenesis of zebrafish by carrying out MO-mediated knock-down of the orthologs of the *mkk4* and *mkk7* genes. We found that *mkk4a* MO-injected zebrafish embryos had no phenotype (Fig. S4B,C), whereas *mkk4b* MO-injected embryos exhibited axial tissues that were abnormally short and wide due to defective CE

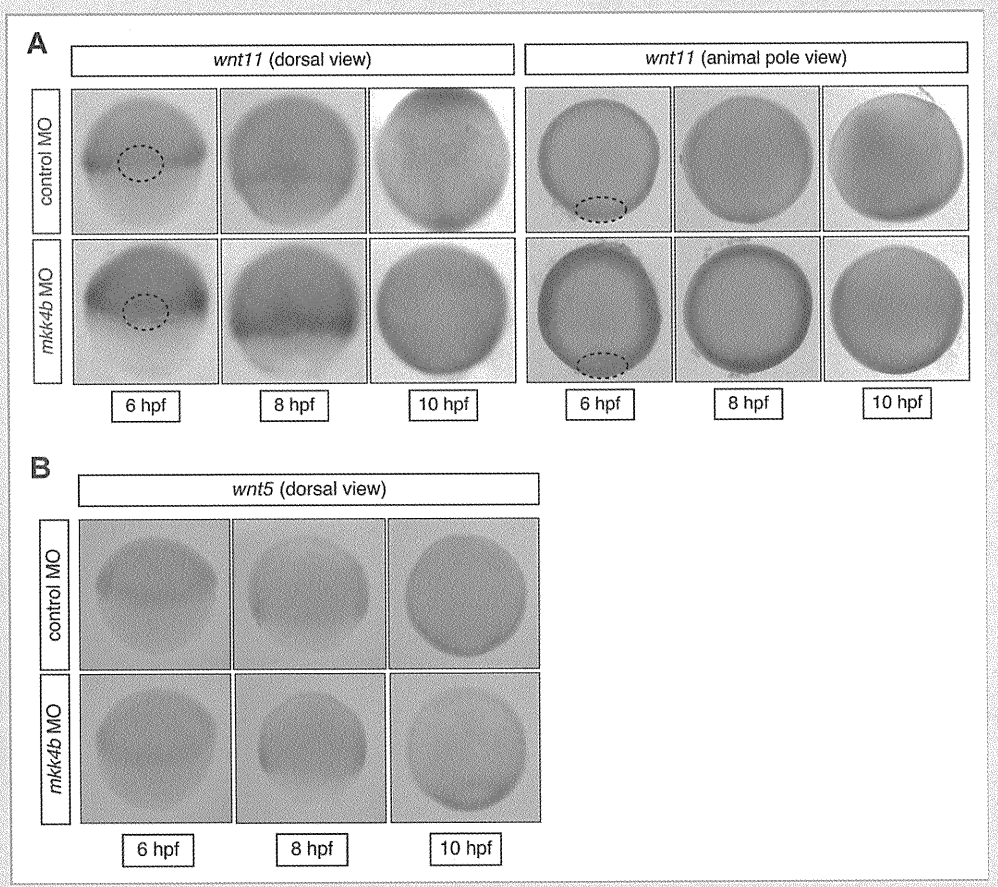

Fig. 6. Elevated expression of *wnt11* in the organizer and margin regions of Mkk4b-depleted embryos. A: Localization of increased *wnt11* expression in *mkk4b* morphants. Whole-mount in situ hybridization was used to monitor *wnt11* expression in developing control and *mkk4b* morphants from the shield stage (6 hpf) to tailbud stage (10 hpf). Two views are shown as indicated, with dashed lines outlining the boundaries of the organizer region. B: Localization of *wnt5* expression in *mkk4b* morphants. Whole-mount in situ hybridization was used to monitor *wnt5* expression in developing control and *mkk4b* morphants from the shield stage (6 hpf) to tailbud stage (10 hpf). *Wnt5* showed the same expression pattern in control and *mkk4b* morphants.

(Fig. 2B–E). These observations suggest that Mkk4b is functionally redundant with Mkk4a and can compensate for its loss during gastrulation, but that Mkk4a cannot compensate for a lack of Mkk4b. *Mkk7* morphants had no phenotype during gastrulation but showed abnormal somite morphologies during segmentation (Fig. 2H–J). Mkk7 is thus critical for a slightly later stage of development.

Recently, Rui et al. [2007] demonstrated that zebrafish *mkk4a-s* plays an important role in dorsoventral patterning in zebrafish blastulas. These authors reported that *mkk4a-s* knockdown with a translation-blocking MO prior to gastrulation reduced the expression of dorsal markers but expanded the expression of ventral markers. In our study, we performed *mkk4a-l* knockdown with translation-blocking MO but could not detect any alteration to the expression of the dorsal marker *gsc* (Fig. S8). This discrepancy implies that there is functional diversity between the two splicing isoforms of *mkk4a*. The results of our study, together with those of Rui et al., reinforce the idea that Jnk signaling plays multiple roles in major developmental processes, including the specification of the dorsoventral axis, cell movements required during gastrulation, and somite morphogenesis.

Our previous studies of disruption of the *mkk4* and *mkk7* genes in murine ES cells revealed that Mkk4 and Mkk7 preferentially phosphorylate the Tyr and Thr residues, respectively, within the Thr-Pro-Tyr motif of Jnk [Kishimoto et al., 2003]. In this study, we expressed zebrafish Mkk4 and Mkk7 in mouse ES cells and obtained results indicating that these Mapks also differ in their biochemical properties (Fig. 1C). These data strongly suggest that the use of Jnk activation as a molecular switch has been evolutionarily conserved from teleosts to mammals. In zebrafish, loss of Mkk4b leads to severe defects in CE movements during gastrulation, whereas our *mkk7* morphants had no phenotype during gastrulation (Fig. 2D,I). These observations indicate that *mkk4* has a more prominent role than *mkk7* in early embryogenesis. Consistent with this hypothesis, *mkk4*$^{-/-}$ mouse embryos die earlier than *mkk7*$^{-/-}$ embryos [Nishina et al., 1999; Wada et al., 2004]. This conserved functional

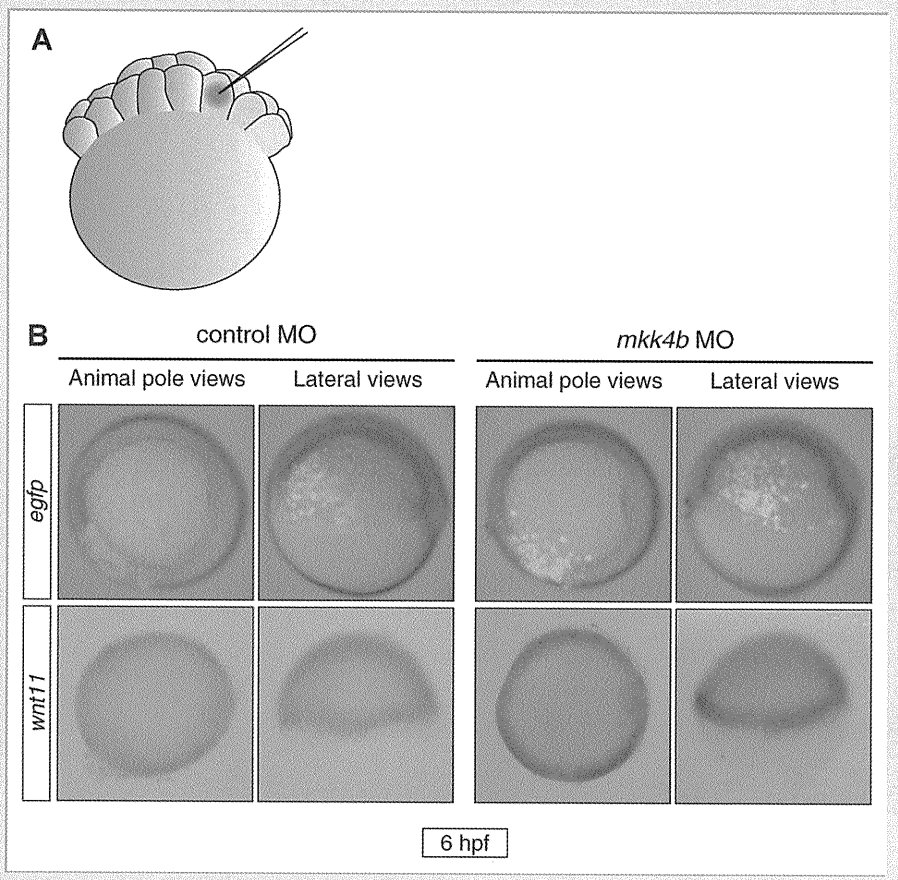

Fig. 7. Abrogation of Mkk4b function induces elevated expression of *wnt11* in a non-cell-autonomous manner. A: Schematic representation of MO microinjection into one cell of a 32- or 64-cell zebrafish embryo. B: Control MO (0.4 pmol) or *mkk4b* MO (0.4 pmol) was injected into one cell of a 32- or 64-cell embryo to generate randomly distributed *mkk4b*-knockdown cell clones. *Egfp* mRNA was co-injected as a cell lineage tracer. Top, EGFP-labeled cells were observed at the shield stage by fluorescence microscopy using a halogen lamp and blue light. Bottom, *wnt11* expression was monitored in developing control and *mkk4b* morphants at the shield stage by whole-mount in situ hybridization. Two views are shown, with dorsal to the right.

diversity of Mapks may be related to the need to activate Jnk at different times and locations during early development. Indeed, we found that Mkk4b depletion reduced Jnk phosphorylation more dramatically than did Mkk7 depletion, at least at the shield stage (Fig. 3B). Alternatively, the functional properties of Mkk4b–Jnk and Mkk7–Jnk signaling modules may be governed in part by scaffold proteins such as the Jnk-interacting proteins (JIPs) that confer specificity to kinase actions [Whitmarsh, 2006].

Jnk1$^{-/-}$*jnk2*$^{-/-}$ mice die at about E11 with defective neural tube morphogenesis [Kuan et al., 1999]. Based on our results in zebrafish, we speculate that the failure to close the neural tube in *jnk1*$^{-/-}$*jnk2*$^{-/-}$ mice may be due to defective CE in the neural plate. In support of this idea, disruption of non-canonical Wnt pathway genes (such as *dishevelled*) in *Xenopus* inhibits CE in the neural plate and results in abnormal, widely spaced neural folds that do not close [Copp et al., 2003]. Invertebrate development may also rely on Jnk-mediated events that share molecular similarities with vertebrate CE. In *Drosophila*, dJnk (Basket) is activated by dJnkk (Hemipterous), a homolog of vertebrate Mkk7 [Glise et al., 1995; Riesgo-Escovar et al., 1996; Sluss et al., 1996]. *Basket* and *hemipterous* are important for morphogenesis, and loss of function of either gene inhibits dorsal closure [Glise et al., 1995; Riesgo-Escovar et al., 1996; Sluss et al., 1996]. These findings emphasize the notion that Jnk activation is utilized in parallel morphogenetic events among widely divergent species.

Signals initiated by non-canonical Wnt ligands such as Wnt11 and Wnt5 are important for: vertebrate morphogenetic processes that require directed cell movements; cell–cell adhesion; and the establishment of cell polarity. Zebrafish with mutations in *wnt5* (*ppt*) or *wnt11* (*slb*) exhibit defects that reduce CE without affecting cell fate [Heisenberg et al., 2000; Kilian et al., 2003]. The *slb* mutant shows more anterior CE defects, including a shortened and broadened body axis at the end of gastrulation and a slight fusion of the eyes (cyclopia) at later developmental stages. In contrast, the Wnt5 protein functions in posterior regions. The *ppt* mutant exhibits a shortened body axis and compressed tail, whereas the position of the eyes is only mildly affected. These observations indicate that Wnt11 and Wnt5 possess distinct and non-redundant functions in regulating zebrafish gastrulation, which may be accounted for by differences in spatiotemporal expression. Although both *wnt5* and

wnt11 are expressed in the germ ring at the shield stage, *wnt11* is specifically expressed in anterior tissues at the end of gastrulation, whereas *wnt5* is specifically expressed in posterior mesendodermal tissues (Fig. 6) [Heisenberg et al., 2000; Kilian et al., 2003]. Our study demonstrates that Mkk4b–Jnk signaling precisely regulates *wnt11* transcription. This Mkk4b–Jnk-mediated control may contribute to the mechanisms segregating *wnt11* and *wnt5* expression domains during late gastrulation.

In *Drosophila*, a role for Dpp in dorsal closure during early morphogenesis has been clearly established [Hou et al., 1997; Riesgo-Escovar and Hafen, 1997]. During dorsal closure, Jnk activates the expression of *dpp* in leading-edge epithelial cells, and Dpp subsequently acts as a secreted signal that controls the elongation of lateral epidermis in a paracrine fashion [Reed et al., 2001]. Our analyses demonstrate that Mkk4b–Jnk signaling regulates *wnt11* expression during zebrafish gastrulation in a non-cell-autonomous manner (Fig. 7). Our results raise the possibility that, like *Drosophila* dorsal closure, normal vertebrate CE movements depend on Jnk signaling that regulates the expression of a secreted signaling molecule capable of promoting concerted movements of neighboring cells (Fig. S7).

Our proposed model of CE movement regulation by *wnt11* expression can be summarized as follows: In normal zebrafish embryos, activated Mkk4b transmits a signal leading to Jnk activation. This activated Jnk may induce secreted factor X, which exerts moderate suppression of *wnt11* transcription in neighboring organizer and margin cells, and results in proper co-ordination of CE. In *mkk4b* morphants, however, JNK activation is blocked such that the expression of factor X is downregulated. As a result, *wnt11* is expressed at an abnormally high level that may impair CE (Fig. 7). We undertook preliminary studies to examine whether the *mkk4b* morphant phenotype could be suppressed by a low dose of *wnt11* MO, but found that rescue did not occur (data not shown). This inability to rescue the CE defect may be due to a failure to strictly control the expression pattern and amount of *wnt11* expression, since Wnt11 levels and localization must be tightly regulated for normal embryonic development [Heisenberg et al., 2000].

A previous study demonstrated that Bmp activity regulates CE movements during zebrafish gastrulation [Myers et al., 2002]. This report prompted us to investigate whether zebrafish Bmp2 and Bmp4 (homologs of *Drosophila* Dpp) function downstream of the Mkk4b–Jnk signaling cascade. However, expression levels of *bmp2* and *bmp4* were not downregulated in Mkk4b-depleted embryos (data not shown). Future identification of secreted factor(s) responsible for the transmission of Jnk signals to neighboring cells may provide insight into the complex mechanisms controlling vertebrate CE.

Our proposed model postulates that *wnt11* expression is under precise spatiotemporal control during zebrafish development. Previous studies have shown that Wnt11 expression in zebrafish starts in the dorsal part of the blastoderm margin at the oblong stage, and that the entire margin becomes $Wnt11^+$ by the late blastula stage [Makita et al., 1998]. Our present work shows that, at the onset of gastrulation, *wnt11* is highly expressed around the circumference of the germ ring, with slightly reduced expression in the region of the organizer (Fig. 6A). It has been established that *wnt11* is expressed predominantly in epiblast cells of the germ ring (ectodermal germ layer), whereas ingressing hypoblast cells (mesendodermal germ layer) show no detectable *wnt11* expression [Makita et al., 1998; Ulrich et al., 2003]. This profile of early *wnt11* expression in zebrafish is virtually identical to that seen in *Xenopus* [Ku and Melton, 1993]. Taken together, these results suggest an evolutionary conservation of *wnt11* function during gastrulation, and a prominent role for the control of *wnt11* expression by Jnk signaling.

ACKNOWLEDGMENTS

We thank numerous members of the Nishina and Katada Laboratories for their helpful discussions and critical comments on the manuscript. This work was partly supported by a Grant-in-Aid for Scientific Research on a Priority Area from the Ministry of Education, Culture, Sports, Science and Technology of Japan. This work was also supported by grants from the Japan Society for the Promotion of Science, the Ministry of Education, Culture, Sports, Science and Technology of Japan, and the Ministry of Health, Labor and Welfare of Japan.

REFERENCES

Asaoka Y, Mano H, Kojima D, Fukada Y. 2002. Pineal expression-promoting element (PIPE), a cis-acting element, directs pineal-specific gene expression in zebrafish. Proc Natl Acad Sci USA 99:15456–15461.

Chang L, Karin M. 2001. Mammalian MAP kinase signalling cascades. Nature 410:37–40.

Copp AJ, Greene ND, Murdoch JN. 2003. Dishevelled: Linking convergent extension with neural tube closure. Trends Neurosci 26:453–455.

Davis RJ. 2000. Signal transduction by the JNK group of MAP kinases. Cell 103:239–252.

Derijard B, Hibi M, Wu IH, Barrett T, Su B, Deng T, Karin M, Davis RJ. 1994. JNK1: A protein kinase stimulated by UV light and Ha-Ras that binds and phosphorylates the c-Jun activation domain. Cell 76:1025–1037.

Fleming Y, Armstrong CG, Morrice N, Paterson A, Goedert M, Cohen P. 2000. Synergistic activation of stress-activated protein kinase 1/c-Jun N-terminal kinase (SAPK1/JNK) isoforms by mitogen-activated protein kinase kinase 4 (MKK4) and MKK7. Biochem J 352(Pt 1): 145–154.

Ganiatsas S, Kwee L, Fujiwara Y, Perkins A, Ikeda T, Labow MA, Zon LI. 1998. SEK1 deficiency reveals mitogen-activated protein kinase cascade cross-regulation and leads to abnormal hepatogenesis. Proc Natl Acad Sci USA 95:6881–6886.

Glise B, Bourbon H, Noselli S. 1995. Hemipterous encodes a novel *Drosophila* MAP kinase kinase, required for epithelial cell sheet movement. Cell 83:451–461.

Habas R, Kato Y, He X. 2001. Wnt/Frizzled activation of Rho regulates vertebrate gastrulation and requires a novel Formin homology protein Daam1. Cell 107:843–854.

Habas R, Dawid IB, He X. 2003. Coactivation of Rac and Rho by Wnt/Frizzled signaling is required for vertebrate gastrulation. Genes Dev 17:295–309.

Heisenberg CP, Tada M, Rauch GJ, Saude L, Concha ML, Geisler R, Stemple DL, Smith JC, Wilson SW. 2000. Silberblick/Wnt11 mediates convergent extension movements during zebrafish gastrulation. Nature 405:76–81.

Hou XS, Goldstein ES, Perrimon N. 1997. *Drosophila* Jun relays the Jun amino-terminal kinase signal transduction pathway to the Decapentaplegic signal transduction pathway in regulating epithelial cell sheet movement. Genes Dev 11:1728–1737.

Kallunki T, Su B, Tsigelny I, Sluss HK, Derijard B, Moore G, Davis R, Karin M. 1994. JNK2 contains a specificity-determining region responsible for efficient c-Jun binding and phosphorylation. Genes Dev 8:2996–3007.

Keller R. 2002. Shaping the vertebrate body plan by polarized embryonic cell movements. Science 298:1950–1954.

Kilian B, Mansukoski H, Barbosa FC, Ulrich F, Tada M, Heisenberg CP. 2003. The role of Ppt/Wnt5 in regulating cell shape and movement during zebrafish gastrulation. Mech Dev 120:467–476.

Kim GH, Han JK. 2005. JNK and ROKalpha function in the noncanonical Wnt/RhoA signaling pathway to regulate Xenopus convergent extension movements. Dev Dyn 232:958–968.

Kimmel CB, Ballard WW, Kimmel SR, Ullmann B, Schilling TF. 1995. Stages of embryonic development of the zebrafish. Dev Dyn 203:253–310.

Kishimoto H, Nakagawa K, Watanabe T, Kitagawa D, Momose H, Seo J, Nishitai G, Shimizu N, Ohata S, Tanemura S, Asaka S, Goto T, Fukushi H, Yoshida H, Suzuki A, Sasaki T, Wada T, Penninger JM, Nishina H, Katada T. 2003. Different properties of SEK1 and MKK7 in dual phosphorylation of stress-induced activated protein kinase SAPK/JNK in embryonic stem cells. J Biol Chem 278:16595–16601.

Ku M, Melton DA. 1993. Xwnt-11: A maternally expressed Xenopus wnt gene. Development 119:1161–1173.

Kuan CY, Yang DD, Samanta Roy DR, Davis RJ, Rakic P, Flavell RA. 1999. The Jnk1 and Jnk2 protein kinases are required for regional specific apoptosis during early brain development. Neuron 22:667–676.

Lawler S, Fleming Y, Goedert M, Cohen P. 1998. Synergistic activation of SAPK1/JNK1 by two MAP kinase kinases in vitro. Curr Biol 8:1387–1390.

Link V, Shevchenko A, Heisenberg CP. 2006. Proteomics of early zebrafish embryos. BMC Dev Biol 6:1.

Makita R, Mizuno T, Koshida S, Kuroiwa A, Takeda H. 1998. Zebrafish wnt11: Pattern and regulation of the expression by the yolk cell and No tail activity. Mech Dev 71:165–176.

Mohit AA, Martin JH, Miller CA. 1995. p493F12 kinase: A novel MAP kinase expressed in a subset of neurons in the human nervous system. Neuron 14:67–78.

Myers DC, Sepich DS, Solnica-Krezel L. 2002. Bmp activity gradient regulates convergent extension during zebrafish gastrulation. Dev Biol 243:81–98.

Nishina H, Fischer KD, Radvanyi L, Shahinian A, Hakem R, Rubie EA, Bernstein A, Mak TW, Woodgett JR, Penninger JM. 1997. Stress-signalling kinase Sek1 protects thymocytes from apoptosis mediated by CD95 and CD3. Nature 385:350–353.

Nishina H, Vaz C, Billia P, Nghiem M, Sasaki T, De la Pompa JL, Furlonger K, Paige C, Hui C, Fischer KD, Kishimoto H, Iwatsubo T, Katada T, Woodgett JR, Penninger JM. 1999. Defective liver formation and liver cell apoptosis in mice lacking the stress signaling kinase SEK1/MKK4. Development 126:505–516.

Nishitai G, Shimizu N, Negishi T, Kishimoto H, Nakagawa K, Kitagawa D, Watanabe T, Momose H, Ohata S, Tanemura S, Asaka S, Kubota J, Saito R, Yoshida H, Mak TW, Wada T, Penninger JM, Azuma N, Nishina H, Katada T. 2004. Stress induces mitochondria-mediated apoptosis independent of SAPK/JNK activation in embryonic stem cells. J Biol Chem 279:1621–1626.

Okuda Y, Yoda H, Uchikawa M, Furutani-Seiki M, Takeda H, Kondoh H, Kamachi Y. 2006. Comparative genomic and expression analysis of group B1 sox genes in zebrafish indicates their diversification during vertebrate evolution. Dev Dyn 235:811–825.

Reed BH, Wilk R, Lipshitz HD. 2001. Downregulation of Jun kinase signaling in the amnioserosa is essential for dorsal closure of the *Drosophila* embryo. Curr Biol 11:1098–1108.

Riesgo-Escovar JR, Hafen E. 1997. *Drosophila* Jun kinase regulates expression of decapentaplegic via the ETS-domain protein Aop and the AP-1 transcription factor DJun during dorsal closure. Genes Dev 11:1717–1727.

Riesgo-Escovar JR, Jenni M, Fritz A, Hafen E. 1996. The *Drosophila* Jun-N-terminal kinase is required for cell morphogenesis but not for DJun-dependent cell fate specification in the eye. Genes Dev 10:2759–2768.

Rui Y, Xu Z, Xiong B, Cao Y, Lin S, Zhang M, Chan SC, Luo W, Han Y, Lu Z, Ye Z, Zhou HM, Han J, Meng A, Lin SC. 2007. A beta-catenin-independent dorsalization pathway activated by Axin/JNK signaling and antagonized by aida. Dev Cell 13:268–282.

Seifert JR, Mlodzik M. 2007. Frizzled/PCP signalling: A conserved mechanism regulating cell polarity and directed motility. Nat Rev Genet 8:126–138.

Shinya M, Eschbach C, Clark M, Lehrach H, Furutani-Seiki M. 2000. Zebrafish Dkk1, induced by the pre-MBT Wnt signaling, is secreted from the prechordal plate and patterns the anterior neural plate. Mech Dev 98:3–17.

Sluss HK, Han Z, Barrett T, Goberdhan DC, Wilson C, Davis RJ, Ip YT. 1996. A JNK signal transduction pathway that mediates morphogenesis and an immune response in *Drosophila*. Genes Dev 10:2745–2758.

Solnica-Krezel L. 2005. Conserved patterns of cell movements during vertebrate gastrulation. Curr Biol 15:R213–R228.

Tada M, Concha ML, Heisenberg CP. 2002. Non-canonical Wnt signalling and regulation of gastrulation movements. Semin Cell Dev Biol 13:251–260.

Thisse C, Thisse B, Schilling TF, Postlethwait JH. 1993. Structure of the zebrafish snail1 gene and its expression in wild-type, spadetail and no tail mutant embryos. Development 119:1203–1215.

Tournier C, Dong C, Turner TK, Jones SN, Flavell RA, Davis RJ. 2001. MKK7 is an essential component of the JNK signal transduction pathway activated by proinflammatory cytokines. Genes Dev 15:1419–1426.

Ulrich F, Concha ML, Heid PJ, Voss E, Witzel S, Roehl H, Tada M, Wilson SW, Adams RJ, Soll DR, Heisenberg CP. 2003. Slb/Wnt11 controls hypoblast cell migration and morphogenesis at the onset of zebrafish gastrulation. Development 130:5375–5384.

Ura S, Nishina H, Gotoh Y, Katada T. 2007. Activation of the c-Jun N-terminal kinase pathway by MST1 is essential and sufficient for the induction of chromatin condensation during apoptosis. Mol Cell Biol 27:5514–5522.

Wada T, Joza N, Cheng HY, Sasaki T, Kozieradzki I, Bachmaier K, Katada T, Schreiber M, Wagner EF, Nishina H, Penninger JM. 2004. MKK7 couples stress signalling to G2/M cell-cycle progression and cellular senescence. Nat Cell Biol 6:215–226.

Watanabe T, Nakagawa K, Ohata S, Kitagawa D, Nishitai G, Seo J, Tanemura S, Shimizu N, Kishimoto H, Wada T, Aoki J, Arai H, Iwatsubo T, Mochita M, Satake M, Ito Y, Matsuyama T, Mak TW, Penninger JM, Nishina H, Katada T. 2002. SEK1/MKK4-mediated SAPK/JNK signaling participates in embryonic hepatoblast proliferation via a pathway different from NF-kappaB-induced anti-apoptosis. Dev Biol 250:332–347.

Westerfield M. 1994. The Zebrafish Book: A Guide for the Laboratory Use of Zebrafish (*Branchydanio rerio*), Institute of Neuroscience. Eugene, OR: University of Oregon.

Whitmarsh AJ. 2006. The JIP family of MAPK scaffold proteins. Biochem Soc Trans 34:828–832.

Whitmarsh AJ, Cavanagh J, Tournier C, Yasuda J, Davis RJ. 1998. A mammalian scaffold complex that selectively mediates MAP kinase activation. Science 281:1671–1674.

Yamanaka H, Moriguchi T, Masuyama N, Kusakabe M, Hanafusa H, Takada R, Takada S, Nishida E. 2002. JNK functions in the non-canonical Wnt pathway to regulate convergent extension movements in vertebrates. EMBO Rep 3:69–75.

Yamashita S, Miyagi C, Fukada T, Kagara N, Che YS, Hirano T. 2004. Zinc transporter LIVI controls epithelial-mesenchymal transition in zebrafish gastrula organizer. Nature 429:298–302.

Yang D, Tournier C, Wysk M, Lu HT, Xu J, Davis RJ, Flavell RA. 1997. Targeted disruption of the MKK4 gene causes embryonic death, inhibition of c-Jun NH2-terminal kinase activation, and defects in AP-1 transcriptional activity. Proc Natl Acad Sci USA 94:3004–3009.

Retinoic Acid Signaling Positively Regulates Liver Specification by Inducing *wnt2bb* Gene Expression in Medaka

Takahiro Negishi,[1,2] Yoko Nagai,[1,2] Yoichi Asaoka,[1] Mami Ohno,[1] Misako Namae,[1] Hiroshi Mitani,[3] Takashi Sasaki,[4] Nobuyoshi Shimizu,[4] Shuji Terai,[5] Isao Sakaida,[5] Hisato Kondoh,[6,7] Toshiaki Katada,[2] Makoto Furutani-Seiki,[6,8*] and Hiroshi Nishina[1*‡]

During vertebrate embryogenesis, the liver develops at a precise location along the endodermal primitive gut tube because of signaling delivered by adjacent mesodermal tissues. Although several signaling molecules have been associated with liver formation, the molecular mechanism that regulates liver specification is still unclear. We previously performed a screen in medaka to isolate mutants with impaired liver development. The medaka *hio* mutants exhibit a profound (but transient) defect in liver specification that resembles the liver formation defect found in zebrafish *prometheus* (*prt*) mutants, whose mutation occurs in the *wnt2bb* gene. In addition to their liver abnormality, *hio* mutants lack pectoral fins and die after hatching. Positional cloning indicated that the *hio* mutation affects the *raldh2* gene encoding retinaldehyde dehydrogenase type2 (RALDH2), the enzyme principally responsible for retinoic acid (RA) biosynthesis. Mutations of *raldh2* in zebrafish preclude the development of pectoral fins. Interestingly, in *hio* mutants, expression of *wnt2bb* in the lateral plate mesoderm (LPM) directly adjacent to the liver-forming endoderm was completely lost. *Conclusion:* Our data reveal the unexpected finding that RA signaling positively regulates the *wnt2bb* gene expression required for liver specification in medaka. These results suggest that a common molecular mechanism may underlie liver and pectoral fin specification during piscine embryogenesis. (HEPATOLOGY **2010;51:1037-1045.**)

Embryonic liver development occurs in multiple stages that are governed by hormonal factors as well as by intercellular and matrix–cellular interactions. In mice, liver ontogeny initiates on approximately embryonic day 9 (E9), when epithelial cells of the foregut endoderm interact with the cardiogenic mesoderm and commit to becoming the liver primordium. The liver primordium proliferates and invades the mesenchyme of the septum transversum to give rise to the hepatic codes and bud at E9.5.[1,2] Over the last decade, studies in rats and mice have greatly expanded the list of molecules known to contribute to liver development;

Abbreviations: AP, anteroposterior; atRA, all-trans retinoic acid; ck19, cytokeratin19; cp, ceruloplasmin; E, embryonic day; hio, hiohgi; LPM, lateral plate mesoderm; MO, Morpholino; mRNA, messenger RNA; nls, neckless; nof, no-fin; PED6, N-([6-(2,4-dinitro-phenyl)amino]hexanoyl)-1-palmitoyl-2-BODIPY-FL-pentanoyl-sn-glycero-3-phosphoethanolamine; prt, prometheus; RA, retinoic acid; RALDH2, Retinaldehyde dehydrogenase type2.

From the [1]Department of Developmental and Regenerative Biology, Medical Research Institute, Tokyo Medical and Dental University, Tokyo, Japan; the [2]Department of Physiological Chemistry, Graduate School of Pharmaceutical Sciences, University of Tokyo, Tokyo, Japan; the [3]Department of Integrated Biosciences, Graduate School of Frontier Science, University of Tokyo, Chiba, Japan; the [4]Department of Molecular Biology, Keio University School of Medicine, Tokyo, Japan; the [5]Department of Gastroenterology & Hepatology, Yamaguchi University Graduate School of Medicine, Yamaguchi, Japan; the [6]Japan Science and Technology Agency, Solution Oriented Research for Science and Technology Kondoh Research Team, Kyoto, Japan; the [7]Department of Frontier Biosciences, Graduate School of Frontier Biosciences, Osaka University, Osaka, Japan; and the [8]Centre for Regenerative Medicine, Department of Biology and Biochemistry, University of Bath, Bath, UK.

Received August 11, 2009; accepted October 9, 2009.

Supported by Grants-in-Aid for Scientific Research from the Ministry of Education, Culture, Sport, Science and Technology of Japan and the Ministry of Health, Labor and Welfare of Japan.

Address reprint requests to: Hiroshi Nishina, Department of Developmental and Regenerative Biology, Medical Research Institute, Tokyo Medical and Dental University, 1-5-45, Yushima, Bunkyo-ku, Tokyo 113-8510, Japan. E-mail: nishina.dbio@mri.tmd.ac.jp; fax: (81)-3-5803-5829.

Published online in Wiley InterScience (www.interscience.wiley.com).

DOI 10.1002/hep.23387

Potential conflict of interest: Nothing to report.

Additional Supporting Information may be found in the online version of this article.

however, it is likely that many more factors are involved in this complex process. In particular, the mechanism underlying the local induction of liver formation remains poorly understood. This gap in our knowledge is reflected in the dearth of reports on rodent mutations that specifically interfere with the initial specification of the liver anlage.

Small fish are particularly suitable for mutational investigations because they are easy to rear in a relatively compact space, their generation times are reasonably short, and they produce transparent embryos. In many fish species, embryos develop outside the mother's body, making it easy to inspect them visually and to manipulate their tissues and cells. Our group has previously used systematic mutagenesis in medaka to generate numerous mutations affecting various aspects of liver development and function.[3-5] The focus of this paper is the recessive mutation *hiohgi* (*hio*). In wild-type (WT) medaka, the hepatic bud forms from the endoderm rod at stage 25 (50 hours post-fertilization at 27°C; 18-19 somite stage).[6] In medaka *hio* embryos, the liver does not appear until stage 29 and is small and malformed. In addition to this liver defect, *hio* mutant embryos lack pectoral fins and die after hatching. These phenotypes suggested to us that the study of *hio* mutants might allow the dissection of various aspects of embryonic specification and perhaps the linking of liver formation to fin formation.

The signaling pathway of vertebrate limb formation has been studied in detail.[7] Limbs arise from regions of the lateral plate mesoderm (LPM) at specific positions along the main anteroposterior (AP) body axis. A number of studies have shown that the limb-inducing signal originates in the axial mesoderm and is relayed from there to the LPM. In mouse, chick, and zebrafish, this signal is thought to be retinoic acid (RA), the bulk of which is synthesized by retinaldehyde dehydrogenase type2 (RALDH2) in early somites and the LPM.[8-15] With respect to downstream effectors, molecular studies have clearly shown that RA signaling from the zebrafish somitic mesoderm leads to the expression of the *wnt2ba* gene in the intermediate mesoderm, which then signals to the LPM and triggers *tbx5* expression. *Tbx5* is required for Fgf signaling in the fin bud that leads to *prdm1* expression, which in turn triggers *fgf10* and *bmp2b* expression.[7,16]

In contrast, the identity of an initial hepatic inducer in vertebrates has yet to be validated genetically. In the first report to isolate a single gene regulating vertebrate liver specification, Ober et al.[17] characterized an interesting zebrafish mutant called *prometheus* (*prt*). In *prt* embryos, the liver is absent or greatly reduced in size at 50 hours post-fertilization but may start to develop and "catch up" to normal size at a later stage. Positional cloning and further analysis revealed that the *prt* mutation altered the *wnt2bb* gene (the second *wnt2b* gene) and that *prt/wnt2bb* was expressed in restricted bilateral domains in the LPM directly adjacent to the liver-forming endoderm. Subsequently, Shin et al.[18] reported that Fgf and Bmp signaling pathways play important roles in zebrafish liver specification and raised the possibility that these molecules act downstream of Wnt2bb. However, the molecules that act upstream of Wnt2bb during liver specification remain to be identified.

In this study, we carried out a detailed characterization of our medaka *hio* mutants, whose signature phenotypes are a small liver and no pectoral fins. Our results define *hio* as a missense mutation of the *raldh2* gene, the expression of which likely results in a nonfunctional RALDH2 protein that cannot support fin development. We also show that the *hio* mutation causes a retardation of liver budding that resembles that observed in zebrafish *prt* mutants, and that *wnt2bb* expression is undetectable in *hio* LPM. Our data suggest that the role of RA signaling in the specification of both liver and fins is to induce expression of *wnt2b* family genes.

Materials and Methods

Fish Maintenance. Medaka were raised and maintained under standard laboratory conditions at approximately 27°C. Heterozygous carriers of the *hio* mutation were identified by random intercrosses. To obtain homozygous *hio* mutant embryos, heterozygous carriers of the *hio* mutation were mated. Typically, the eggs were spawned synchronously every morning. Embryos were raised at 30°C, and embryonic stages were determined based on morphological features, as previously described.[6]

Genetic Mapping. The *hio* mutation was induced in the Cab-Kyoto line of medaka.[3] The Kaga-Kyoto line of medaka was used for polymorphic marker-based genetic mapping.[3] Genetic mapping and chromosome walking were performed essentially as described.[19]

Reverse-Transcription Polymerase Chain Reaction and Gene Segment Alignment. Partial or full-length complementary DNAs of the *raldh2* (Accession number AB439727), *tbx5* (AB439834), *wnt2bb* (AB439835), *wnt2ba*, *cp*, *prox1*, *insulin*, and *tbx3* genes were generated by reverse-transcription polymerase chain reaction of messenger RNAs (mRNAs) from various stages of medaka embryos (Supporting Table 1). Alignment was performed using MultAlin (http://prodes.toulouse.inra.fr/multalin/multalin.html).

Injection of mRNA. WT *raldh2* mRNA (400 pg), obtained by *in vitro* transcription of a pBS-KS(−)-*raldh2*

clone, was injected into the cytoplasm of one-cell stage embryos that were the progeny of intercrossed *hio* heterozygotes.

Gene Knockdown by Morpholinos. Morpholino oligonucleotides (MOs) were synthesized by Gene-Tools, LLC (Corvallis, OR). MOs (0.8 pmol) were injected into the cytoplasm of one-cell stage WT medaka embryos. The sequences of MOs used were as follows:

raldh2 MO, 5′-ATGACTGCCGTGGCTGCGCT-GCTGT-3′;

wnt2bb MO, 5′-ATATACCTGAGAGTGTCCA-GAACAG-3′.

Retinoic Acid Treatments. Embryos resulting from *hio* heterozygote intercrosses were incubated in the dark from stage 21 onward in various dilutions of a 10^{-2} M all-*trans* RA (Sigma) stock solution in dimethylsulfoxide. The diluent was 1× balanced salt solution composed of 110 mM NaCl, 5 mM KCl, 1 mM $CaCl_2$, and 2.2 mM $MgSO_4$, pH7.5. Teratogenic effects (such as disrupted heart and AP axis) were observed at 10^{-8} M all-*trans* RA and above.

Whole-Mount* In Situ *Hybridization. Whole-mount *in situ* hybridization was performed as previously described,[3] using antisense DIG-labeled riboprobes generated from medaka *tbx5*, *wnt2ba*, *prox1*, *cp*, *insulin*, *wnt2bb*, *tbx3*, or *raldh2* partial or full-length complementary DNAs. Probes used to detect *gata6*, *foxA3*, *ck19*, and *pdx1* expression were as previously described.[4]

N-([6-(2,4-Dinitro-Phenyl) Amino] Hexanoyl)-1-Palmitoyl-2-BODIPY-FL-Pentanoyl-sn-Glycero-3-Phosphoethanolamine–Mediated Tracking of Lipid Metabolism. Medaka embryos at stage 36 were placed in 0.5 mL 1× balanced salt solution containing 0.3 mg/mL N-([6-(2,4-dinitro-phenyl)amino]hexanoyl)-1-palmitoyl-2-BODIPY-FL-pentanoyl-*sn*-glycero-3-phosphoethanolamine (PED6) and incubated in the dark for 4 hours at 28°C. The treated embryos were rinsed with 1× balanced salt solution and placed in a glass depression slide. PED6 fluorescence was detected using a Zeiss Axioplan 2 microscope.

Results

The* hio *Mutation Alters the* raldh2 *Gene. Using bulked segregation analysis, we performed positional cloning and mapped hio between restriction fragment length polymorphisms OLc2806f and Scaf21_1.0M on LG3 (Fig. 1A). This region includes a sequence with homology to the mammalian and zebrafish *raldh2* genes. Because the "missing fin" phenotype of medaka *hio* mutants was similar to that of the zebrafish *raldh2* mutants *neckless* (*nls*) and *no-fin* (*nof*),[8,10] *raldh2* appeared to be a good candidate for the gene affected by the *hio* mutation. We compared the sequence of a genomic fragment encoding the WT medaka *raldh2* gene with the sequences of the corresponding fragments from four independent homozygous *hio* embryos. We found an A to G transversion in *hio* alleles that would cause the threonine 468 residue in the WT RALDH2 enzyme to be replaced by alanine (Fig. 1B). A comparison of the predicted WT RALDH2 amino acid sequences among medaka, human, xenopus, and zebrafish revealed an overall amino acid sequence identity of 81% (between medaka and human or xenopus) and 84% (between medaka and zebrafish) (Fig. 1C). The threonine 468 residue was conserved among all species examined. Moreover, threonine 468 lies within the catalytic domain of WT RALDH2 (Fig. 1C). These results suggest that the mutant RALDH2 protein produced in *hio* mutants is inactive.

It has been well established that the defects of RA signaling lead to the impairment of fin development in zebrafish.[7,8,10,16] We showed that the injection of *RALDH2*-MO into WT embryos results in the impairment of fin development, and the injection of *raldh2* mRNA or exogenous RA rescued the defects of fin development of *hio* mutant (Supporting Fig. 1). These results indicate that RALDH2 and RA regulate fin development in medaka. In addition, *hio* embryos lacked *tbx5* and *wnt2ba* expression, which acted downstream of RA during fin development (Supporting Fig. 2). Taken together, we concluded that RA signaling plays important roles in fin development in medaka.

Loss-of-Function of RALDH2 Reduces Liver Size in Medaka. We have previously reported that the medaka *hio* mutation results in a small and malformed liver.[3] To examine the role of *raldh2*-dependent signaling in liver formation in medaka, we employed three approaches. First, to investigate whether loss-of-function of *raldh2* could account for this liver defect, we injected *raldh2*-MO into WT embryos and inspected the developing liver. We found that the *raldh2* morphants had the same undersized livers as the *hio* mutants (Fig. 2A). Estimation of liver size via *in situ* hybridization using a *gata6* probe confirmed the reduced liver size in the *raldh2* morphants (Fig. 2B). Second, to determine whether the *hio*/*raldh2* mutation was responsible for the small livers of these mutants, we injected *in vitro* transcribed *raldh2* mRNA into the cytoplasm of one-cell stage embryos that were the progeny of intercrossed *hio* heterozygotes and used *gata6 in situ* hybridization to assay these embryos for rescue of liver size. As expected, 25% of the progeny of intercrossed *hio* heterozygotes (uninjected controls) had small livers. In contrast, the percentage of progeny with

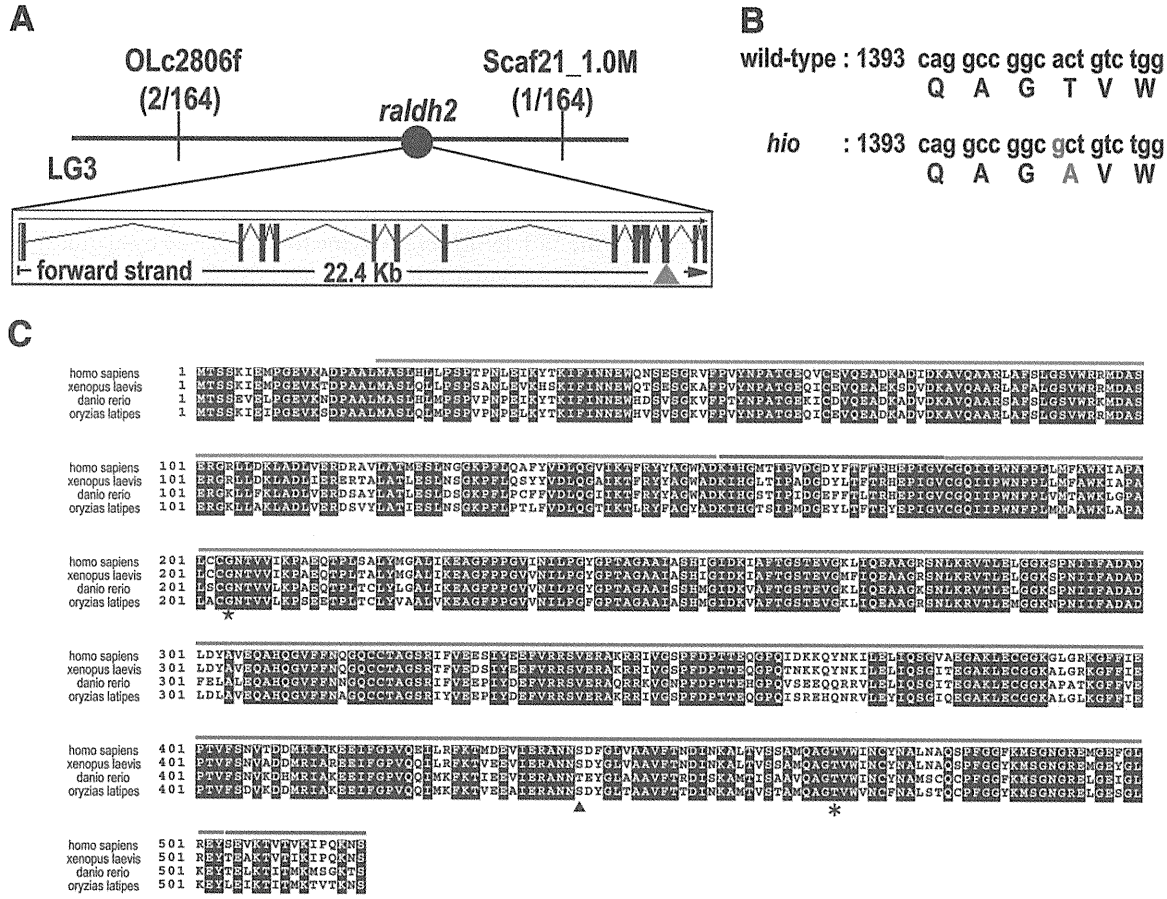

Fig. 1. Mapping and cloning of medaka *hio/raldh2*. (A) Genetic map of the locus affected by the *hio* mutation and the exon/intron structure of the medaka *raldh2* gene. The position of the *hio* mutation is indicated by the red triangle. (B) Comparison of the medaka WT *raldh2* and *hio* nucleotide sequences (lower case) and the corresponding deduced RALDH2 amino acid sequences (upper case). The *hio* mutation and the amino acid it affects are shown in red. (C) Alignment of the deduced amino acid sequences of RALDH2 proteins in *Homo sapiens* (Accession number BAA34785), *Xenopus laevis* (AAG32057), *Danio rerio* (zebrafish; AAL00899), and *Oryzias latipes* (medaka; AB439727). Residues on a black background are conserved among all four species. Red, green, and blue horizontal lines indicate the RALDH2 catalytic domain (289-503), nucleotide binding domain (20-154, 179-288), and tetramerization domain (155-178, 504-518), respectively.[29] The asterisk indicates the position of the *hio* mutation (T468A) in medaka. The star and triangle indicate the positions of the zebrafish *nls* (G204R) and *nof* (T441K) mutations, respectively.

decreased liver size was reduced to 14% after injection of *raldh2* mRNA (Fig. 2C). Finally, we investigated whether treatment with exogenous RA, the bulk of which is synthesized by RALDH2, could rescue the liver defects caused by the *hio* mutation. We treated the progeny of intercrossed *hio* heterozygotes with all-*trans* retinoic acid (atRA) and monitored liver development. Whereas 25% of the untreated progeny of intercrossed *hio* heterozygotes had small livers, the percentage of progeny with a small liver was reduced to 13% after exposure to 5×10^{-9} M atRA (Fig. 2D). Thus, treatment with either WT *raldh2* mRNA or exogenous RA can rescue the small liver phenotype in at least some *hio* mutants, although the efficiency of such rescue is much lower for the liver than for the pectoral fin. When the livers of *hio* mutants with treatment with either WT *raldh2* mRNA or exogenous RA became as large as that of WT medaka, we judged it to be rescued. Therefore, we may have underestimated the recovery rate of liver phenotype. In any case, the loss of *raldh2* function in *hio* mutants causes a defect not only in pectoral fin development but also in liver formation.

The* hio *Mutation Retards Liver Specification. Although the molecular mechanism by which RA signaling initiates fin development is well established,[7,20] the molecular regulation of liver development by RA signaling remains to be elucidated. To address this issue, we used *in situ* hybridization with a probe specific for the endodermal marker *foxA3* to monitor liver development in *hio* embryos. Whereas hepatic buds were observed in WT medaka at stage 25, these structures did not form in *hio* mutants until stage 29 (Fig. 3A). By stage 32, hepatic buds were noticeably smaller in *hio* embryos compared

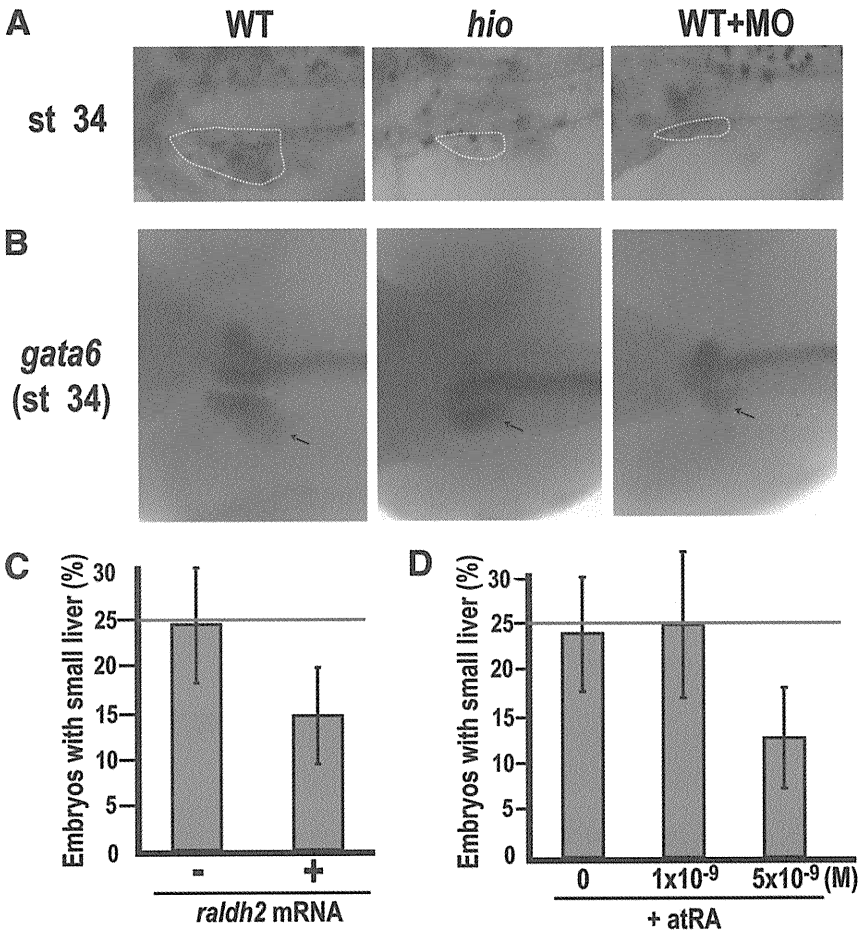

Fig. 2. Impaired liver formation in *hio* embryos is attributable to loss of *raldh2* function. (A) Lateral views of WT, *hio* mutant, and *raldh2* morphant (MO) embryos at stage 34. Dotted lines highlight the liver region. (B) Whole-mount *in situ* hybridization to detect *gata6* expression in WT, *hio* mutant, and *raldh2* morphant (MO) embryos at stage 34. Arrows indicate the liver region. For A-C, images shown are one example representative of more than 10 embryos examined per group. (C) Rescue of the *hio* mutation by *raldh2* mRNA. Progeny one-cell embryos of intercrossed *hio* heterozygotes were injected with *raldh2* mRNA (n = 49), and liver development was monitored. In the absence of *raldh2* mRNA (n = 50), the expected 25% (red line) of progeny (*hio* homozygotes) showed impaired liver development. Bars indicate the mean ± standard error. (D) Rescue of the *hio* mutation by all-*trans* retinoic acid (atRA) treatment. Progeny one-cell embryos of intercrossed *hio* heterozygotes were treated with the indicated concentrations of atRA (0 M; n = 50, 1×10^{-9} M; n = 32, 5×10^{-9} M; n = 39), and liver development was monitored. In the absence of 5×10^{-9} M atRA, the expected 25% (red line) of progeny (*hio* homozygotes) showed impaired liver development. Bars indicate the mean ± standard error.

with the WT. These data indicate that the medaka *hio* mutation retards hepatic bud formation.

Next, we determined whether the *hio* mutation interferes with the initial specification of liver anlage in medaka. We carried out *in situ* hybridization using a probe for the hepatic specification marker *prox1* to monitor liver specification. In WT medaka embryos, *prox1* was induced in the hepatic bud starting at stage 25 (Fig. 3B, upper panel), and by stage 29, *prox1*-positive cells were observed only in the hepatic region. In *hio* embryos, the formation of the hepatic bud was delayed until stage 29 (Fig. 3A), so that *prox1*-positive cells were not observed in the hepatic region until this stage (Fig. 3B, bottom panel). These results indicate that the *hio* mutation compromises the signaling pathway required for initial hepatic fate specification.

The Small Livers in* hio *Embryos Exhibit Normal Hepatic Cell Differentiation and Function. The most important cell types in the vertebrate liver are cholangiocytes (bile duct cells) and hepatocytes. To determine whether hio livers were capable of normal hepatic cell differentiation, we subjected WT and *hio* embryos to *in situ* hybridization with a probe for the cholangiocyte marker *cytokeratin19* (*ck19*) and the hepatocyte marker *ceruloplasmin* (*cp*). At stage 28, although WT embryos showed a few *ck19*-positive cells in the hepatic region, *hio* embryos did not (Supporting Fig. 3). However, by stage 32, *ck19* expression was comparable in WT and *hio* livers (Fig. 4A, left panel). Furthermore, *cp* expression was comparable in WT and *hio* livers at stage 34 (Fig. 4A, right panel). Thus, although liver formation is delayed in *hio* embryos, the small livers of these mutants can give rise to differentiated liver cells. To ascertain whether the small *hio* liver was functional, we took advantage of a reporter system based on PED6, a fluorescent phospholipid.[21] When WT medaka ingest PED6, endogenous lipase activity and the rapid transport of cleavage products results in intense gallbladder fluorescence.[4] We observed equivalent levels of green fluorescence in the gallbladders of WT and *hio* embryos treated with PED6 at stage 36 (Fig. 4B), indicating that *hio* livers have a normal capacity to metabolize lipids. Taken together, our results show that loss of *raldh2* function initially impairs liver specification and retards liver development but does not impair hepatic

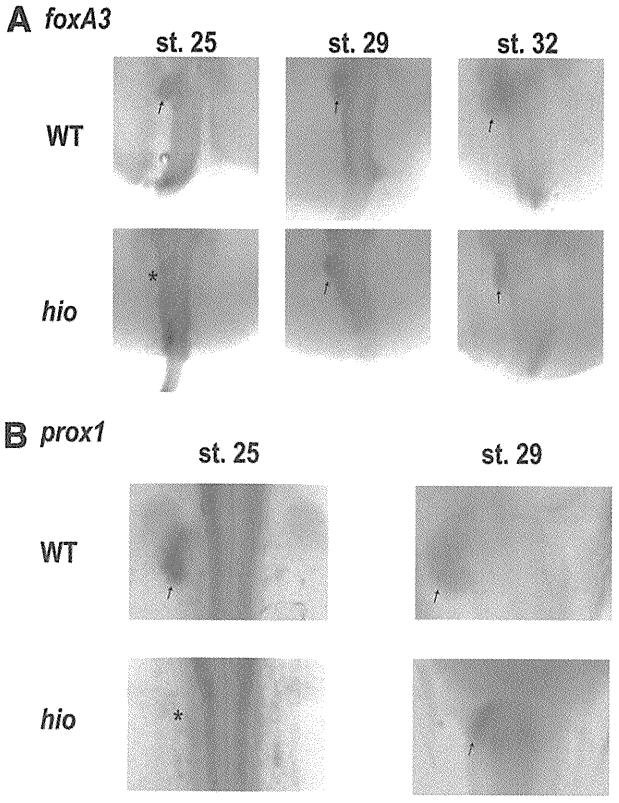

Fig. 3. Impaired hepatic bud formation but normal pancreas in *hio* embryos. (A) Whole-mount *in situ* hybridization to detect *foxA3* expression in WT and *hio* mutant embryos at stages 25, 29, and 32. Arrows indicate hepatic buds derived from the foregut. Asterisk indicates that no hepatic bud is present in the *hio* mutant at stage 25. (B) Whole-mount *in situ* hybridization to detect *prox1* expression in WT and *hio* mutant embryos at stages 25 and 29. Arrows indicate hepatic region. Asterisk indicates that no *prox*1 expression is observed in the *hio* mutant at stage 25. For A and B, images shown are single examples representative of more than 20 embryos examined per group.

cell differentiation or liver functions at later stages of embryogenesis.

Stafford and Prince[22] have reported that hepatic and pancreatic cell markers are undetectable in zebrafish *nls* embryos. To investigate whether the *hio* mutation affected pancreas development in medaka, we carried out *in situ* hybridization using probes for the *pdx1* and *insulin* genes. We observed *pdx1*-expressing cells in the pancreatic primordium region in both WT and *hio* embryos at stage 28 (Fig. 4C). Furthermore, *insulin*-expressing cells were present in both WT and *hio* embryos at stage 30 (Fig. 4D). Thus, unlike its effects on liver development, the medaka *hio* mutation does not appear to affect pancreas development. This result stands in contrast to the zebrafish *nls* mutation, which severely impairs the development of both the liver and the pancreas.

wnt2bb *Expression in the LPM Is Lost in* hio *Embryos.* It has been shown in zebrafish that mesodermal *wnt2bb* expression promotes liver specification.[17] It is also known that the *wnt2ba* gene acts downstream of RA signaling and regulates pectoral fin development in zebrafish.[7,20] The *wnt2ba* and *wnt2bb* genes are both members of *wnt2b* gene family that exists in both zebrafish and medaka. These observations suggested to us that Wnt2bb might be a good candidate for the key molecule regulating piscine liver specification downstream of RA signaling. To explore this hypothesis, we examined *wnt2bb* expression in *hio* embryos. At stage 22, no *wnt2bb* expression in the LPM was observed in either WT or *hio* embryos (Supporting Fig. 4). However, by stage 24, *wnt2bb* expression in the LPM directly adjacent to the liver-forming endoderm was induced in WT embryos but not in *hio* embryos (Fig. 5A, left panel). These results suggest that the *hio* mutation causes a loss of *wnt2bb* gene

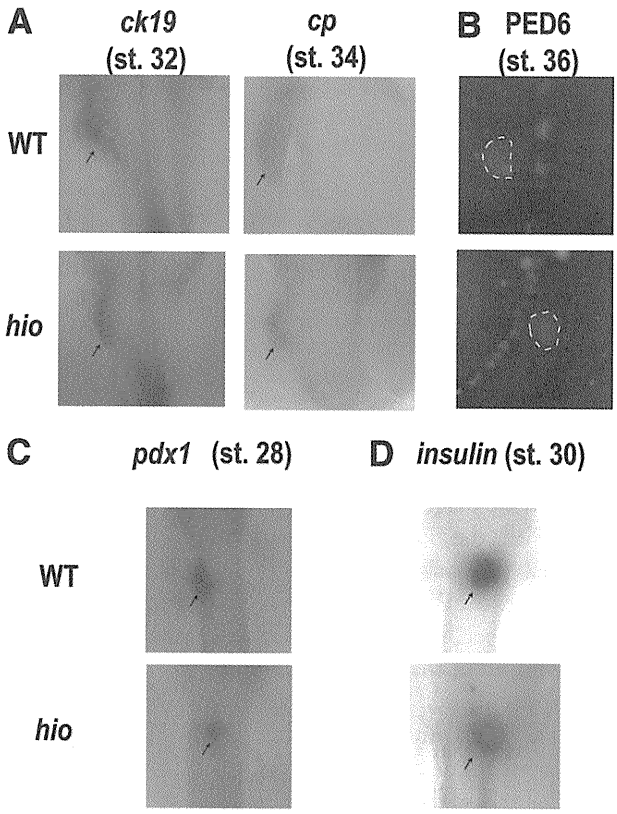

Fig. 4. Normal hepatic cell differentiation and function and pancreatic development in *hio* embryos. (A) Whole-mount *in situ* hybridization of WT and *hio* mutant embryos to detect *ck19* expression by cholangiocytes at stage 32, and *cp* expression by hepatocytes at stage 34. Arrows indicate *ck19*-positive or *cp*-positive livers. (B) WT and *hio* mutant embryos at stage 36 were treated with PED6 to assay liver lipid metabolism. White dashed lines indicate green fluorescence attributable to PED6 metabolites. (C) Whole-mount *in situ* hybridization to detect *pdx1* expression (arrows) in WT and *hio* mutant embryos at stage 28. (D) Whole-mount *in situ* hybridization to detect *insulin* expression (arrows) in WT and *hio* mutant embryos at stage 30. For A-D, images shown are single examples representative of more than 10 embryos examined per group.

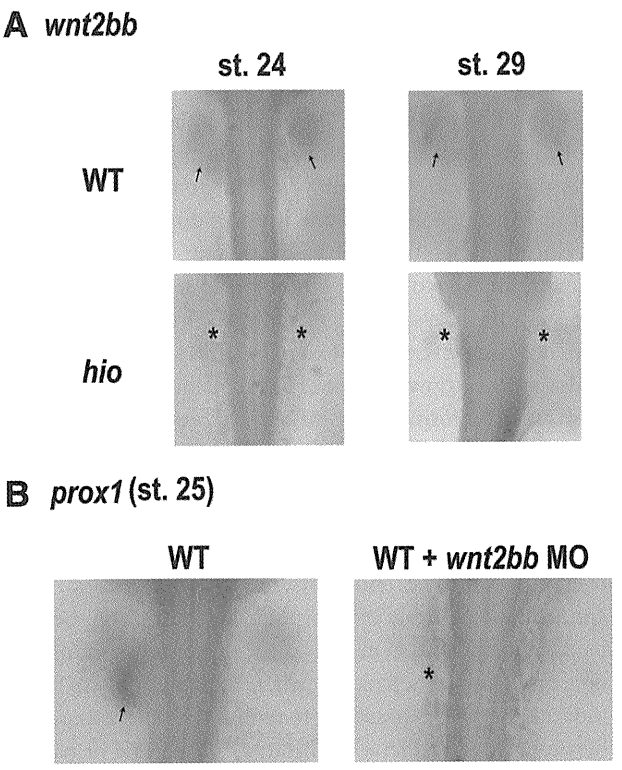

Fig. 5. Impaired *wnt2bb* expression in *hio* embryos. (A) Whole-mount *in situ* hybridization to detect *wnt2bb* expression in WT and *hio* mutant embryos at stages 24 and 29. Arrows indicate *wnt2bb* expression in the WT. Asterisks indicate the lack of *wnt2bb* expression in *hio* mutant embryos. (B) Whole-mount *in situ* hybridization to detect *prox1* expression in WT and *wnt2bb*-morphant (MO) embryos at stage 25. Arrow indicates *prox1* expression in the WT hepatic region. Asterisk indicates the lack of *prox1* expression in the MO embryo. Images shown are single examples representative of more than 20 embryos examined per group.

expression. Interestingly, *wnt2bb* still had not been expressed in the *hio* LPM at stage 29, when the liver bud forms (Fig. 5A, right panel). Thus, the small livers that eventually appear in medaka *hio* mutants seem to form independently of Wnt2bb signaling, just as occurs in zebrafish *prt* mutants.

To investigate whether *wnt2bb* positively regulates liver specification in medaka as it does in zebrafish, we injected *wnt2bb*-specific morpholino antisense oligonucleotides (*wnt2bb*-MO) into the cytoplasm of one-cell stage WT embryos and evaluated the outcome by *in situ* hybridization using a *prox1* probe. We found that, like *hio* embryos, WT medaka embryos that had been injected with *wnt2bb*-MO lacked *prox1* expression (Fig. 5B). These results suggest that Wnt2bb signaling is responsible for liver specification in medaka.

In conclusion, our study has shown that the *hio* mutation in medaka impairs liver specification by abrogating *wnt2bb* expression. Our data are thus the first genetic evidence that RA signaling positively regulates liver specification by inducing *wnt2bb* expression.

Discussion

Function of RA Signaling in Pectoral Fin and Liver Development in Medaka. In this study, we examined the role of RA signaling during embryogenesis by characterizing medaka *hio* mutants. These mutants bear an alteration to the *raldh2* gene (Fig. 1) that encodes the enzyme principally responsible for RA synthesis, and we interpret that this is a nearly null mutation because the phenotypes of *hio* mutant are similar to that of RALDH2 morphants (Fig. 2 and Supporting Fig. 1). The *hio* mutants exhibit two prominent phenotypes: missing pectoral fins and a small liver (Fig. 2 and Supporting Fig. 1). Work in mouse, chick, and zebrafish has shown that RA signaling from the somitic mesoderm is essential for limb induction and is mediated by the expression of downstream factors such as *wnt2ba* and *tbx5*.[7-14] We show that the *hio* mutation in medaka leads to defects in pectoral fin development and *tbx5* and *wnt2ba* expression (Supporting Fig. 2). Thus, our results indicate that RA signaling is crucial for fin specification in medaka and show that limb induction signaling is conserved across a broad range of species (Fig. 6, right part). Significantly, our work has also uncovered a role for RA signaling in liver development. We have demonstrated that the *hio* mutation retards the formation of hepatic buds from the foregut (Fig. 3A) and causes a profound defect in liver specification (Fig. 3B). In addition, we have shown that the *wnt2bb* expression required for the regulation of liver specification is undetectable in the LPM of *hio* embryos (Fig. 5A). Our data constitute the first genetic evidence that RA signaling regulates vertebrate liver specification by inducing *wnt2bb* gene expression (Fig. 6, left part). Previously, Wang et al.[23] reported that liver growth is severely affected in RALDH2-deficient mouse embryos. Thus, RA signaling in liver specification may be conserved among other species.

Molecular Mechanisms Regulating the Development of Pectoral Fins and Liver. There are several similarities in the signaling pathways governing pectoral fin and liver organogenesis. During zebrafish pectoral fin development, RA signaling induces *wnt2ba* expression, which in turn induces *tbx5* expression. *Tbx5* is a key molecule that regulates the expression of downstream effectors such as the *fgf* and *bmp* family members *fgf24*, *fgf10*, and *bmp2b*.[7,16] Thus, limb induction requires a sequential RA → Wnt → Tbx → Fgf + Bmp signaling cascade. A parallel situation may exist for liver specification in medaka. Wnt2bb, Tbx3, Fgf, and Bmp have all been shown to positively regulate the development of this organ in mice or zebrafish.[17,18,24] In this study, we showed

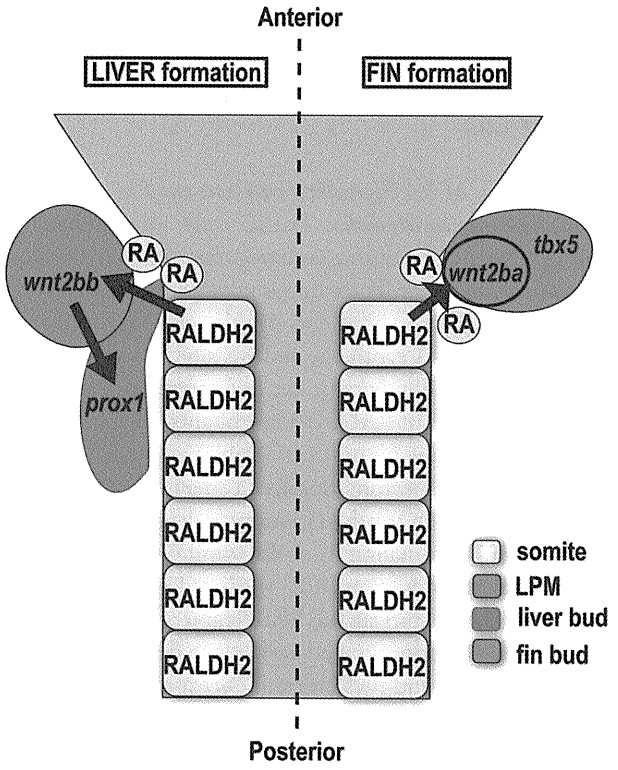

Fig. 6. Schematic model of RA signaling during liver and pectoral fin formation in a WT medaka embryo. (Left) During liver formation in medaka, RALDH2 expression in the somites results in the production of RA that induces *wnt2bb* expression. This Wnt2bb then induces *prox1* expression in the liver bud, which in turn drives hepatocyte migration.[30] (Right) During fin formation, RALDH2 expression in the somites results in the production of RA that induces *wnt2ba* and *tbx5* expression in the fin bud that drives fin cell differentiation.

that RALDH2 drives *wnt2bb* expression during liver specification in medaka (Fig. 5). Based on the proposal of Shin et al.[18] that Fgf and Bmp act downstream of Wnt2bb during liver specification, the sum total of all these results suggests that liver specification also requires a sequential RA → Wnt → Fgf + Bmp signaling cascade. Intriguingly, we found that RA signaling induced *tbx3* expression in medaka (Supporting Fig. 5). However, our morpholino studies showed that RA signaling associated with liver formation can regulate *tbx3* expression without involving Wnt2bb (Supporting Fig. 5). These data indicate that Tbx3 can act downstream of RA signaling, but it is likely that other T-box family members are involved in the putative RA → Wnt → Tbx → Fgf + Bmp signaling cascade that drives liver development. We are continuing our search for the identity of this transcription factor.

Differential Requirements for Liver and Pectoral Fin Specification During Embryogenesis. A sequential RA → Wnt → Tbx → Fgf + Bmp signaling cascade is indispensable for the limb induction process that underlies pectoral fin development. Alterations in *raldh2* such as the medaka *hio* and zebrafish *nls* and *nof* mutations lead to an absence of pectoral fins, as does knockdown of *wnt2ba* using MO in WT zebrafish.[8,10,16] Notably, these mutants and morphants never form pectoral fins during the entire course of embryogenesis. Conversely, a sequential RA → Wnt → Fgf + Bmp signaling cascade is not indispensable for liver specification, because medaka *hio* mutants and zebrafish *prt* mutants are able to form a functional liver at an abnormally late stage of development. A molecule that may be able to partially compensate for a loss of RALDH2 is Fgf10, which is also induced downstream of RA signaling and involved in limb and liver formation. Loss of *fgf10* prevents fin development in zebrafish,[7] and Fgf10-deficient mouse embryos lack limbs and have an abnormally small liver.[25,26] Thus, *fgf10* and *raldh2* functions may cooperate during embryogenesis such that their mutation results in similar phenotypes. Moreover, in zebrafish *fgf10* mutants, the hepatopancreatic ductal epithelium is severely dysmorphic, and cells of the hepatopancreatic ductal system and adjacent intestine misdifferentiate and adopt a hepatic or pancreatic fate.[27] These results indicate that Fgf10 functions to repress the differentiation of hepatopancreatic ductal epithelium into hepatic or pancreatic cells and thus demarcates developing organs and tissues. In our *hio* mutants, it may be that the observed lack of liver specification leads not only to impaired liver development but also to misdifferentiation in the hepatopancreatic ductal system that results in the formation of a small liver. Such misdifferentiation could obscure an absolute requirement of *raldh2* for liver specification, and might create an obstacle to finding mutations that specifically interfere with the initial specification of the liver anlage. Further analysis is needed to substantiate this hypothesis.

Comparison of* raldh2 *Alterations in Medaka* hio *and Zebrafish* nls *Mutants. The nls mutation in zebrafish is a loss-of-function allele of the *raldh2* gene that was generated by the ENU approach. Originally, *nls* was isolated in an *in situ* hybridization screen and was detected by its effects on neural AP patterning.[8] The *nls* embryos lack pectoral fin buds and fins. A similar phenotype has been reported for a natural loss-of-function *raldh2* mutation in zebrafish called *no-fin*.[10] In addition to their lack of fins, *nls* embryos do not express the hepatocyte and pancreatic cell markers that are detectable in WT zebrafish embryos.[22] Stafford and Prince[22] also showed that exogenous RA treatment of WT zebrafish embryos resulted in the anterior expansion of the pancreatic anlage. Thus, RA signaling is a determinant of the regionalization of both neuroectoderm and endoderm, and defects in *raldh2* function prevent the development of the endodermal region in which liver and pancreatic cells would normally appear. In contrast, our medaka *hio* mutation does not have severe effects on neuroectoderm and

endoderm regionalization, and the liver in *hio* embryos, although reduced in size and delayed in appearance, eventually forms in the normal location. Thus, *hio* is a unique mutation affecting liver organogenesis, and continued study of this mutation should yield new insights into the involvement of RA signaling in liver specification. It remains to be elucidated how medaka *hio* mutants escape the defect in endodermal regionalization associated with zebrafish *nls* mutations.

The availability of two closely related fish model systems, medaka and zebrafish, for studies in genetics, experimental embryology, and molecular biology is unique among vertebrates and advantageous for two reasons. First, the evolutionary distance between these two species is particularly well suited for comparative functional genomics. Second, and more importantly, the parallel existence of medaka and zebrafish transforms the perceived weakness of studying genetics in fish, namely, the many analogous groups of genes formed because of genomic duplications, into an advantage: the study of a gene in one species may shed light on a gene function that is hidden in the other species.[28] For example, RALDH2's function in AP patterning is not apparent in medaka *hio* mutants, and RALDH2's function in liver specification is not apparent in zebrafish *nls* mutants. Our results clearly demonstrate that a comparison of two related species can be a powerful means of dissecting genetic and molecular mechanisms underlying vertebrate development.

Acknowledgment: The authors thank numerous members of the Nishina and Katada laboratories for excellent fish care, technical assistance, and helpful discussions.

References

1. Zaret KS. Hepatocyte differentiation: from the endoderm and beyond. Curr Opin Genet Dev 2001;11:568-574.
2. Zaret KS. Regulatory phases of early liver development: paradigms of organogenesis. Nat Rev Genet 2002;3:499-512.
3. Furutani-Seiki M, Sasado T, Morinaga C, Suwa H, Niwa K, Yoda H, et al. A systematic genome-wide screen for mutations affecting organogenesis in Medaka, Oryzias latipes. Mech Dev 2004;121:647-658.
4. Watanabe T, Asaka S, Kitagawa D, Saito K, Kurashige R, Sasado T, et al. Mutations affecting liver development and function in Medaka, Oryzias latipes, screened by multiple criteria. Mech Dev 2004;121:791-802.
5. Hata S, Namae M, Nishina H. Liver development and regeneration: from laboratory study to clinical therapy. Dev Growth Differ 2007;49:163-170.
6. Iwamatsu T. Stages of normal development in the medaka Oryzias latipes. Mech Dev 2004;121:605-618.
7. Mercader N, Fischer S, Neumann CJ. Prdm1 acts downstream of a sequential RA, Wnt and Fgf signaling cascade during zebrafish forelimb induction. Development 2006;133:2805-2815.
8. Begemann G, Schilling TF, Rauch GJ, Geisler R, Ingham PW. The zebrafish neckless mutation reveals a requirement for raldh2 in mesodermal signals that pattern the hindbrain. Development 2001;128:3081-3094.
9. Berggren K, McCaffery P, Drager U, Forehand CJ. Differential distribution of retinoic acid synthesis in the chicken embryo as determined by immunolocalization of the retinoic acid synthetic enzyme, RALDH-2. Dev Biol 1999;210:288-304.
10. Grandel H, Lun K, Rauch GJ, Rhinn M, Piotrowski T, Houart C, et al. Retinoic acid signalling in the zebrafish embryo is necessary during pre-segmentation stages to pattern the anterior-posterior axis of the CNS and to induce a pectoral fin bud. Development 2002;129:2851-2865.
11. Mic FA, Molotkov A, Molotkova N, Duester G. Raldh2 expression in optic vesicle generates a retinoic acid signal needed for invagination of retina during optic cup formation. Dev Dyn 2004;231;270-277.
12. Niederreither K, McCaffery P, Drager UC, Chambon P, Dolle P. Restricted expression and retinoic acid-induced downregulation of the retinaldehyde dehydrogenase type 2 (RALDH-2) gene during mouse development. Mech Dev 1997;62:67-78.
13. Niederreither K, Subbarayan V, Dolle P, Chambon P. Embryonic retinoic acid synthesis is essential for early mouse post-implantation development. Nat Genet 1999;21:444-448.
14. Stratford TH, Kostakopoulou K, Maden M. Hoxb-8 has a role in establishing early anterior-posterior polarity in chick forelimb but not hindlimb. Development 1997;124:4225-4234.
15. Linville A, Gumusaneli E, Chandraratna RA, Schilling TF. Independent roles for retinoic acid in segmentation and neuronal differentiation in the zebrafish hindbrain. Dev Biol 2004;270:186-199.
16. Ng JK, Kawakami Y, Buscher D, Raya A, Itoh T, Koth CM, et al. The limb identity gene Tbx5 promotes limb initiation by interacting with Wnt2b and Fgf10. Development 2002;129:5161-5170.
17. Ober EA, Verkade H, Field HA, Stainier DY. Mesodermal Wnt2b signalling positively regulates liver specification. Nature 2006;442:688-691.
18. Shin D, Shin CH, Tucker J, Ober EA, Rentzsch F, Poss KD, et al. Bmp and Fgf signaling are essential for liver specification in zebrafish. Development 2007;134:2041-2050.
19. Morinaga C, Saito D, Nakamura S, Sasaki T, Asakawa S, Shimizu N, et al. The hotei mutation of medaka in the anti-Mullerian hormone receptor causes the dysregulation of germ cell and sexual development. Proc Natl Acad Sci U S A 2007;104:9691-9696.
20. Wakahara T, Kusu N, Yamauchi H, Kimura I, Konishi M, Miyake A, et al. Fibin, a novel secreted lateral plate mesoderm signal, is essential for pectoral fin bud initiation in zebrafish. Dev Biol 2007;303:527-535.
21. Farber SA, Pack M, Ho SY, Johnson ID, Wagner DS, Dosch R, et al. Genetic analysis of digestive physiology using fluorescent phospholipid reporters. Science 2001;292:1385-1388.
22. Stafford D, Prince VE. Retinoic acid signaling is required for a critical early step in zebrafish pancreatic development. Curr Biol 2002;12:1215-1220.
23. Wang Z, Dolle P, Cardoso WV, Niederreither K. Retinoic acid regulates morphogenesis and patterning of posterior foregut derivatives. Dev Biol 2006;297:433-445.
24. Suzuki A, Sekiya S, Buscher D, Izpisua Belmonte JC, Taniguchi H. Tbx3 controls the fate of hepatic progenitor cells in liver development by suppressing p19ARF expression. Development 2008;135:1589-1595.
25. Sekine K, Ohuchi H, Fujiwara M, Yamasaki M, Yoshizawa T, Sato T, et al. Fgf10 is essential for limb and lung formation. Nat Genet 1999;21:138-141.
26. Berg T, Rountree CB, Lee L, Estrada J, Sala FG, Choe A, et al. Fibroblast growth factor 10 is critical for liver growth during embryogenesis and controls hepatoblast survival via beta-catenin activation. HEPATOLOGY 2007;46:1187-1197.
27. Dong PD, Munson CA, Norton W, Crosnier C, Pan X, Gong Z, et al. Fgf10 regulates hepatopancreatic ductal system patterning and differentiation. Nat Genet 2007;39:397-402.
28. Furutani-Seiki M, Wittbrodt J. Medaka and zebrafish, an evolutionary twin study. Mech Dev 2004;121:629-637.
29. Lamb AL, Newcomer ME. The structure of retinal dehydrogenase type II at 2.7 A resolution: implications for retinal specificity. Biochemistry 1999; 38:6003-6011.
30. Sosa-Pineda B, Wigle JT, Oliver G. Hepatocyte migration during liver development requires Prox1. Nature Genet 2000;25:254-255.

BJ www.biochemj.org

BJ Signal

Biochem. J. (2010) 427, 237–245 (Printed in Great Britain) doi:10.1042/BJ20091011

Filamin associates with stress signalling kinases MKK7 and MKK4 and regulates JNK activation

Kentaro NAKAGAWA*†‡[1], Misato SUGAHARA‡[1], Tokiwa YAMASAKI*‡[1], Hiroaki KAJIHO‡, Shinya TAKAHASHI*‡, Jun HIRAYAMA§, Yasuhiro MINAMI||, Yasutaka OHTA¶, Toshio WATANABE**, Yutaka HATA†, Toshiaki KATADA‡ and Hiroshi NISHINA*[2]

*Department of Developmental and Regenerative Biology, Medical Research Institute, Tokyo Medical and Dental University, 1-5-45 Yushima, Bunkyo-ku, Tokyo 113-8510, Japan, †Department of Medical Biochemistry, Graduate School of Medicine, Tokyo Medical and Dental University, 1-5-45 Yushima, Bunkyo-ku, Tokyo 113-8519, Japan, ‡Department of Physiological Chemistry, Graduate School of Pharmaceutical Sciences, University of Tokyo, 7-3-1 Hongo, Bunkyo-ku, Tokyo 113-0033, Japan, §Medical Top Track Program, Medical Research Institute, Tokyo Medical and Dental University, 1-5-45 Yushima, Bunkyo-ku, Tokyo 113-8510, Japan, ||Department of Physiology and Cell Biology, Graduate School of Medicine, Kobe University, 7-5-1, Kusunoki-cho, Chuo-ku, Kobe 650-0017, Japan, ¶Department of Medicine, Brigham and Women's Hospital, Harvard Medical School, Boston, Massachusetts 02115-2248, U.S.A., and **Department of Biological Sciences, Graduate School of Humanities and Sciences, Nara Women's University, Nara 630-8506, Japan

SAPK/JNK (stress-activated protein kinase/c-Jun N-terminal kinase) belongs to the MAPK (mitogen-activated protein kinase) family and is important in many biological contexts. JNK activation is regulated by phosphorylation of specific tyrosine and threonine residues sequentially catalysed by MKK4 and MKK7, which are both dual-specificity MAPKKs (MAPK kinases). Previously, we reported that tyrosine-phosphorylation of JNK by MKK4 precedes threonine-phosphorylation by MKK7, and that both are required for synergistic JNK activation. In the present study, we identify the actin-binding protein-280 (Filamin A) as a presumed 'binder' protein that can bind to MKK7, as well as to MKK4, connecting them in close proximity. We show that Filamin family members A, B and C interact with MKK4 and MKK7, but not with JNK. Filamin A binds to an N-terminal region (residues 31–60) present in the MKK7γ and MKK7β splice isoforms, but cannot bind to MKK7α which lacks these amino acids. This same N-terminal region is crucial for the intracellular co-localization of MKK7γ with actin stress fibres and Filamin A. Experiments using Filamin-A-deletion mutants revealed that the MKK7-binding region of Filamin A differs from its MKK4-binding region, and that MKK7γ (but not MKK7α) can form a complex with Filamin A and MKK4. Finally, we used Filamin-A-deficient cells to show that Filamin A enhances MKK7 activation and is important for synergistic stress-induced JNK activation *in vivo*. Thus Filamin A is a novel member of the group of scaffold proteins whose function is to link two MAPKKs together and promote JNK activation.

Key words: Filamin, c-Jun N-terminal kinase (JNK), mitogen-activated protein kinase kinase 4 (MKK4), mitogen-activated protein kinase kinase 7 (MKK7), stress-activated protein kinase (SAPK), stress-activated protein kinase/extracellular-signal-regulated kinase kinase 1 (SEK1).

INTRODUCTION

JNK (c-Jun N-terminal kinase) is a member of the family of MAPKs (mitogen-activated protein kinases), which are ubiquitously expressed and evolutionarily conserved. JNK is activated not only by many types of external stress, including changes in osmolarity, heat shock and UV-irradiation, but also by LPA (lysophosphatidic acid) and inflammatory cytokines. Activated JNK phosphorylates the transcription factors c-Jun, Jun D and ATF-2 (activating transcription factor 2) to regulate gene expression governing stress responses. JNK signalling is also involved in the normal physiological processes of cell proliferation, apoptosis, differentiation and cell migration [1,2].

Activation of JNK requires the phosphorylation of the tyrosine and threonine residues located in a threonine-proline-tyrosine motif in the activation loop between regions VII and VIII of the kinase domain. This phosphorylation is catalysed by two dual-specificity kinases, MKK4 (SEK1) and MKK7. MKK4 and MKK7 are MAPKKs (MAPK kinases) that are activated by various MAPKKKs (MAPKK kinases), including MLKs (mixed lineage protein kinases), MEKK1 {MEK [MAPK/ERK (extracellular-signal-regulated kinase) kinase] kinase}, TAK1 [TGF (transforming growth factor)-β-activated kinase 1] and ASK1 (apoptosis signal-regulating kinase) [1,2]. In-depth studies of JNK activation have shown that MKK4 preferentially phosphorylates the tyrosine residue of the threonine-proline-tyrosine motif, whereas MKK7 preferentially phosphorylates the threonine residue. Phosphorylation of both residues *in vitro* results in synergistic activation of JNK [3–5]. We obtained strong *in vivo* support for this latter activation mechanism from our studies of murine ES (embryonic stem) cells bearing disruptions of the *mkk4* and/or *mkk7* genes [6–8]. No JNK activation was observed in *mkk4*$^{-/-}$*mkk7*$^{-/-}$ ES cells [9]. In *mkk7*$^{-/-}$ ES cells, a severe impairment of JNK activation was observed that was accompanied by loss of phosphorylation of the threonine residue of JNK; however, there was no significant reduction in the phosphorylation of the tyrosine residue of JNK. In *mkk4*$^{-/-}$ ES cells, reductions in the phosphorylation of both the tyrosine and threonine residues of JNK were noted. These results indicated

Abbreviations used: Ab, antibody; CT, C-terminus; ES, embryonic stem; GFP, green fluorescent protein; GST, glutathione transferase; HA, haemagglutinin; HEK, human embryonic kidney; JNK, c-Jun N-terminal kinase; JIP, JNK-interacting protein; JLP, JNK-associated leucine-zipper protein; mAb, monoclonal antibody; MAPK, mitogen-activated protein kinase; MAPKK (MKK), MAPK kinase; MAPKKK, MAPKK kinase; MEKK1, MEK [MAPK/ERK (extracellular-signal-regulated kinase) kinase] kinase; MLK, mixed lineage protein kinase; SAPK, stress-activated protein kinase; JSAP1, JNK/SAPK-associated protein 1; TNF, tumour necrosis factor; TRAF2, TNF-receptor-associated factor.

[1] These authors contributed equally to the present study.

[2] To whom correspondence should be addressed (email nishina.dbio@mri.tmd.ac.jp).

that tyrosine phosphorylation by MKK4, followed by threonine phosphorylation by MKK7, leads to synergistic JNK activation in stress-stimulated ES cells. However, the molecular mechanism underlying the sequential phosphorylation of JNK by MKK4 and MKK7 remains to be elucidated.

Recent studies have shown that scaffold proteins mediate the structural and functional organization of a three-tier MAPK activation module which involves a MAPKKK, a MAPKK and a MAPK [10]. These MAPK-specific scaffold proteins link these kinases into a multienzyme complex and provide an insulated physical conduit through which signals from a MAPK can be transmitted to the appropriate spatiotemporal cellular loci. The scaffold proteins then modulate the signalling strength of their cognate MAPK module by regulating the amplitude and duration of signalling. Several scaffold proteins involved in mammalian JNK signalling modules have been identified, including JIP (JNK-interacting protein) 1, JIP2, JSAP1 [JNK/SAPK (stress-activated protein kinase)-associated protein 1]/JIP3, JLP (JNK-associated leucine-zipper protein) and POSH [plenty of SH3s (Src homology 3)] and their various splice variants. JIP1, JIP2 and JSAP1 bind to JNK, MKK7 and various MLKs. JSAP1 associates with JNK, MKK4 and MEKK1, whereas JLP links Max with c-Myc, and JNK with p38, MKK4 or MEKK3. In addition, multiple upstream MAPKKKs can act as scaffold proteins, as well as exert their intrinsic kinase activities. For example, MEKK1 binds to and regulates MKK4. Despite this flexibility, theoretical considerations have dictated that a single JIP-based MAPK module containing MKK4 and MKK7 physically cannot catalyse the sequential phosphorylation of JNK by these kinases [11]. We therefore speculated that additional scaffold molecules must exist that can bind to and connect two sets of complexes, one containing MKK4 and the other containing MKK7. To identify these presumed 'binder' molecules, we used MKK7 and the yeast two-hybrid method to screen a human leucocyte cDNA library. We isolated Filamin A, which has been previously reported to interact with MKK4 [12], as a predicted 'binder' protein that can also interact with MKK7. Our results show that different MKK7 splice isoforms [13] have different scaffold-binding properties, and that Filamin A plays an important role in synergistic JNK activation.

EXPERIMENTAL

Cell culture

HEK (human embryonic kidney)-293T cells, HeLa cells and non-transfected (M2) or stably transfected (A7) human melanoma cell lines were maintained in DMEM (Dulbecco's modified Eagle's medium) supplemented with 10 % FCS (fetal calf serum), 0.16 % $NaHCO_3$ and 0.6 mg · ml^{-1} L-glutamine. To maintain Filamin A expression, A7 cells were cultured in the presence of 0.5 mg/ml G418 (Sigma).

Antibodies and GFP (green fluorescent protein) vector

Abs (antibodies) against human Filamin A (MAB1680) were from Chemicon. Abs against SAPK/JNK1 (C-17 and FL) or phospho-SAPK/JNK (#9251) were from Santa Cruz Biotechnology and Cell Signaling Technology respectively. Anti-FLAG (M2) and anti-c-Myc (9E10) Abs were from Sigma–Aldrich. Anti-HA (haemagglutinin) high-affinity (3F10) Ab was from Roche Diagnostics. The rat anti-MKK7 (KN-004) mAb (monoclonal Ab) used for immunoprecipitation and immunoblotting was prepared in our laboratory as previously described [7]. Abs against MKK4 (sc-837) or phospho-MKK4 (#9151) were from Santa Cruz Biotechnology and Cell Signaling Technology respectively. The pEGFP-C1 vector was from BD Biosciences.

Construction of plasmids

cDNAs encoding FLAG-tagged versions of MKK4, MKK7α1, MKK7β1, MKK7γ1, MKK7γ2, JNK1 and full-length Filamin A were cloned into the mammalian expression vector pCMV5. Plasmids expressing Myc-tagged full-length Filamin A, the Myc-tagged CT (C-terminus) of Filamin A (residues 2282–2647), or Myc–Filamin B, Myc–Filamin C or HA-tagged MKK4 were also cloned into pCMV5. Myc-tagged Filamin A deletion mutants A, B and C were generated using PCR and subcloned into pCMV5. FLAG-tagged MKK7 deletion mutants A, B and C were constructed using a One Day Mutagenesis kit (QuikChange® kit from Stratagene) and cloned into pCMV5.

Transfection

For gene expression analysis, HEK-293T cells were plated at 6×10^6 cells in a 100-mm dish, or at 2×10^6 cells in a 60-mm dish. Cells were transfected 1 day later with 5 μg (100-mm dish) or 1.8 μg (60-mm dish) of plasmid DNA using 5 μl of Lipofectamine™ 2000 (Invitrogen). M2 cells were plated at 1.25×10^6 cells in a 60-mm dish and transfected 1 day later with 2.5 μg of plasmid DNA as above. After 48 h in culture, cell extracts were prepared and subjected to immunoprecipitation as described below.

Immunoprecipitation and immunoblotting

Transfected HEK-293T cells were resuspended in lysis buffer A [20 mM Hepes/KOH (pH 7.4), 40 mM NaCl, 1 % Triton X-100, 1 mM dithiothreitol, 1 mM EDTA, 2 mM EGTA and 0.1 mM PMSF] at 4 °C. Cell lysates were incubated with anti-FLAG M2 agarose (Sigma) at 4 °C for 2 h. The immunocomplexes were washed several times with lysis buffer A and eluted with 200 μg/ml FLAG peptides. The eluted samples were fractionated by SDS/PAGE and proteins were electrophoretically transferred on to a PVDF membrane (Bio-Rad). Membranes were immunoblotted with anti-FLAG, anti-Myc, anti-HA or anti-(Filamin A) Abs. Bands were visualized using SuperSignal West Pico Chemiluminescent Substrate for the development of immunoblots and a HRP (horseradish peroxidase)-conjugated secondary Ab, according to the manufacturer's instructions (Pierce).

Assay of JNK and MKK7 activities

Confluent melanoma cells were treated at 37 °C for 20 min with sorbitol (50, 100, 150, 200, 300 or 500 mM). Treated cells were washed and resuspended in lysis buffer B [100 mM NaCl, 40 mM Tris/HCl (pH 8.0), 1 % Nonidet P40, 0.05 % 2-mercaptoethanol, 1 mM EDTA, 1 mM EGTA and 4 μg/ml aprotinin]. Extracts were incubated for 2 h at 4 °C with anti-JNK pAb (polyclonal antibody; C-17, Santa Cruz Biotechnology) to immunoprecipitate JNK proteins. Endogenous MKK7 proteins were immunoprecipitated in a similar manner with anti-MKK7 (KN-004) mAb. Immunocomplexes were washed three times with lysis buffer B and three times with kinase reaction buffer [10 mM $MgCl_2$, 50 mM Tris/HCl (pH 7.5) and 1 mM EGTA]. JNK activity in immunoprecipitates was measured using a previously described *in vitro* kinase assay [6,7] employing 60 μM [γ-^{32}P]ATP and GST (glutathione transferase)–c-Jun as the substrate. MKK7 activity on beads was measured using an *in vitro* MAPK kinase assay [6,7] employing 100 μM unlabelled ATP with GST–JNK1 as the substrate; the product was detected using an anti-phospho-JNK Ab. For both *in vitro* kinase assays, the reactions were terminated after 30 min at 30 °C by the addition of 10 μl of 4×SDS gel sample buffer.

To assay JNK activity in transfected M2 cells, cells were resuspended in lysis buffer C [150 mM NaCl, 40 mM Hepes (pH 7.4), 1 % Nonidet P40, 0.05 % 2-mercaptoethanol, 1 mM EDTA, 1 mM EGTA, 10 mM $MgCl_2$ and 4 μg/ml aprotinin]. The resulting cell lysates were analysed by SDS/PAGE and immunoblotting in which JNK activation was detected using an anti-phospho-JNK Ab.

Yeast two-hybrid assay

A human brain cDNA library (Clontech) and the MatchMaker™ GAL4 Two-Hybrid System 3 (Clontech) were used, as described previously [14], for a yeast two-hybrid assay in which MKK7 served as the bait.

Confocal microscopy

HeLa cells transiently expressing GFP–MKK7γ1 were cultured on a polylysine-coated glass coverslip (15-mm diameter) and washed three times with PBS before fixation with 4 % (w/v) paraformaldehyde in PBS for 15 min at 4 °C. After treatment with 0.1 mM glycine in PBS for 15 min, the cells were permeabilized with 0.1 % Triton X-100 in blocking solution (3 % BSA in PBS) before incubation for 1 h at room temperature (25 °C) with rhodamine-conjugated phalloidin diluted in blocking solution. After three PBS washes, the coverslip was mounted on to a glass slide in Permafluor-mounting medium (Immunon) and viewed using a confocal microscope (Carl Zeiss) with LSM510 software. Excitation wavelengths of 488 nm or 546 nm were used. The images were merged using Photoshop (Adobe Systems).

For overexpression of GFP-tagged Filamin A, GFP–MKK7α1, GFP–MKK7γ1 or GFP–MKK7 deletion B, and for co-expression of GFP-tagged MKK7γ1 and a fusion protein composed of red fluorescent protein (DsRed) plus Filamin A, transfected HeLa cells were cultured for 48 h in a glass-based dish (35-mm diameter; Iwaki) and examined by confocal microscopy as described previously [14].

RESULTS

Interaction of Filamin A with MKK4 and MKK7

To identify proteins that interacted with both MKK4 and MKK7, a human leucocyte cDNA library was screened with MKK7 in a yeast two-hybrid system. Among various MKK7-binding cDNAs isolated were several encoding the CT of ABP-280 (actin-binding protein-280, Filamin A), which was previously reported to bind to MKK4 [12]. To determine whether endogenous full-length Filamin A could interact with both MKK4 and MKK7 *in vivo*, we transiently overexpressed FLAG–MKK4, FLAG–MKK7γ2 and FLAG–JNK1 in HEK-293T cells and carried out co-immunoprecipitation experiments. As shown in Figure 1(A), a protein of ~280 kDa co-immunoprecipitated with FLAG–MKK4 and FLAG–MKK7γ2, but not with FLAG–JNK1. We confirmed that this 280 kDa protein was indeed Filamin A using Western blotting employing anti-(Filamin A) Ab (Figure 1B). We next used FLAG and Myc tagging to examine whether two other members of the Filamin protein family, Filamin B and Filamin C, could bind to MKK4 and MKK7 *in vivo*. When overexpressed in HEK-293T cells, both Filamin B and Filamin C co-immunoprecipitated with both MKK4 and MKK7γ2 (Figure 1C). These results show that Filamin family proteins can interact with at least two MAPKKs, MKK4 and MKK7γ2, and demonstrate a novel connection between an MKK7 enzyme and a Filamin protein known to interact with MKK4.

Isoform-specific interaction of MKK7 with Filamin A

To date, six isoforms of MKK7 have been identified [12]. To test whether four of these MKK7 isoforms (Figure 2A) interacted differentially with Filamin A, HEK-293T cells were transiently co-transfected with individual FLAG–MKK7 isoforms plus Myc-tagged Filamin A (CT). As shown in Figure 2(B), Myc–Filamin A (CT) co-immunoprecipitated with FLAG–MKK7γ2, FLAG–MKK7γ1 and FLAG–MKK7β1, but not with FLAG–MKK7α1. We next constructed three deletion mutants of MKK7γ1 (MKK7γ1 deletion A, B and C; Figure 2A) that affected the presumed Filamin-A-binding site in MKK7 and repeated the co-immunoprecipitation experiments. Myc–Filamin A (CT) co-immunoprecipitated with FLAG–MKK7γ1 deletion A and deletion C, but not with FLAG–MKK7γ1 deletion B or FLAG–MKK7α1 (Figure 2C). Thus a short N-terminal region (encompassing amino acids 31–60) that is present in MKK7γ and MKK7β, but absent in MKK7α1, is required for MKK7 binding to Filamin A.

Co-localization of MKK7 with Filamin A

To investigate whether MKK7 co-localizes with Filamin A in cells, we first examined the subcellular localization of MKK7γ1 and found that this isoform associated with fibre-like structures. To determine whether these fibres were actin stress fibres, HeLa cells were transiently transfected with GFP-tagged MKK7γ1, fixed, stained with phalloidin to visualize actin distribution, and examined by confocal microscopy. We observed that MKK7γ1 did indeed co-localize with actin stress fibres (Figure 3A). Because Filamin A is known to cross-link actin filaments, these results suggested that MKK7γ1 co-localized with Filamin A. We tested this possibility by transfecting HeLa cells with GFP–MKK7γ1 and DsRed–Filamin A. As expected, MKK7γ1 co-localized with Filamin A in selected areas (Figure 3B). To investigate whether the apparent association of MKK7γ1 with actin stress fibres was due to the interaction of MKK7γ1 with Filamin A, HeLa cells were co-transfected with GFP–Filamin A and GFP–MKK7γ1, GFP–MKK7γ1 deletion B or GFP–phospho-MKK7α1. Confocal microscopy showed that GFP–MKK7γ1 and GFP–Filamin A co-localized on fibre-like structures, whereas GFP–MKK7α1 and GFP–MKK7γ1 deletion B (which do not interact with Filamin A) were diffusely distributed throughout the cytoplasm (Figure 3C). Thus MKK7γ1 and Filamin A co-localize in cells, and MKK7γ1 associates with actin stress fibres due to its interaction with Filamin A.

Filamin A mediates a connection between MKK4 and MKK7γ

The above experiments showed that Filamin A interacts not only with MKK4, but also with MKK7γ and MKKβ isoforms. To identify the regions of Filamin A that can interact with MKK4 or MKK7γ, HEK-293T cells were transiently co-transfected with either Myc–Filamin A (CT), including its MKK4-binding region (amino acids 2282–2454), or a series of Filamin A deletion mutant proteins lacking different portions of the MKK4-binding region (Figure 4A), together with FLAG–MKK4 or FLAG–MKK7γ2. Co-immunoprecipitation assays showed that amino acids 2297–2311 of Filamin A were required for its interaction with MKK7γ2 (Figure 4B). Thus the region of Filamin A required for binding to MKK7γ2 is distinct from that needed for the interaction with MKK4. We then investigated whether Filamin A could interact simultaneously with MKK4 and MKK7γ2 by transiently co-transfecting HEK-293T cells with HA-tagged MKK4 plus FLAG–MKK7γ2 or FLAG–MKK7α1. HA–MKK4

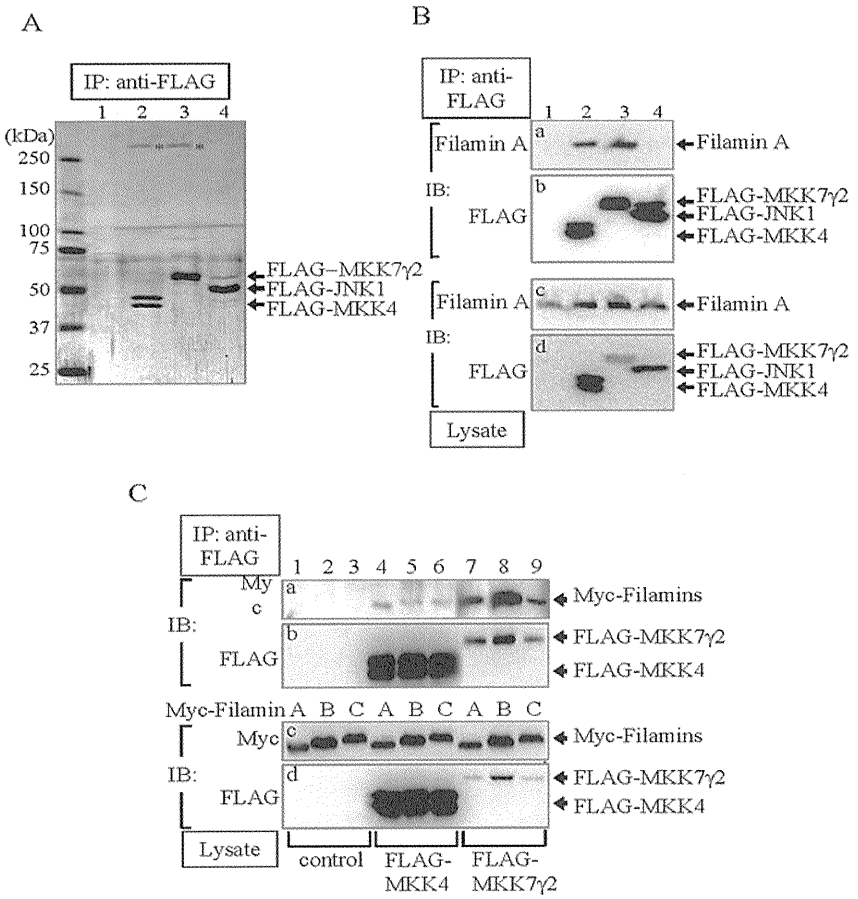

Figure 1 Interaction of Filamin A with MKK4 and MKK7

(**A** and **B**) HEK-293T cells were transfected with 5 μg of pCMV5/FLAG (lanes 1), FLAG–MKK4 (lanes 2), FLAG–MKK7γ2 (lanes 3) or FLAG–JNK1 (lanes 4). Cell lysates were prepared (**B**, panels c and d) and immunoprecipitated (IP) with anti-FLAG M2 agarose (**A** and **B**, panels a and b). (**A**) Co-immunoprecipitated proteins (*) were visualized using Coomassie Blue. The molecular mass in kDa is indicated on the left-hand side. (**B**) Co-immunoprecipitated Filamin A and immunoprecipitated FLAG–MKK4, FLAG–MKK7γ2 and FLAG–JNK1 were identified using anti-(Filamin A) (panel a) and anti-FLAG M2 (panel b) Abs respectively. Expression of Filamin A and FLAG–MKK4, FLAG–MKK7γ2 and FLAG–JNK1 were determined by immunoblotting (IB) using anti-(Filamin A) (panel c) and anti-FLAG M2 (panel d) Abs respectively. (**C**) HEK-293T cells were transfected with 0.9 μg of pCMV5/Myc-Filamin A (CT) (lanes 1, 4 and 7), Myc–Filamin B (lanes 2, 5 and 8) or Myc–Filamin C (lanes 3, 6 and 9), together with 0.9 μg of pCMV5/FLAG (lanes 1–3), FLAG–MKK4 (lanes 4–6) or FLAG–MKK7γ2 (lanes 7–9). Cell lysates were prepared (panels c and d) and immunoprecipitated (IP) with anti-FLAG M2 agarose (panels a and b). Co-immunoprecipitated Myc–Filamin proteins and immunoprecipitated FLAG–MKK4 and FLAG–MKK7γ2 were determined using anti-c-Myc (panel a) and anti-FLAG M2 (panel b) Abs respectively. Expression of Myc–Filamin proteins and FLAG–MKK4 and FLAG–MKK7γ2 were determined using anti-c-Myc (panel c) and anti-FLAG M2 (panel d) Abs respectively. IB, immunoblot.

and endogenous Filamin A co-immunoprecipitated with FLAG–MKK7γ2, but not with FLAG–MKK7α1 (Figure 4C). Because this experiment did not exclude the possibility that MKK4 might interact directly with MKK7γ2 (rather than with Filamin A), we repeated these co-immunoprecipitation experiments using a human melanoma cell line M2 that has spontaneously lost expression of Filamin A [15]. M2 cells were transiently co-transfected with HA–MKK4 and FLAG–MKK7γ2, together with increasing amounts of Myc–Filamin A (CT). Interaction of MKK4 with MKK7 was enhanced when higher amounts of Filamin A (CT) were present (Figure 4D), suggesting that Filamin A, MKK4 and MKK7γ2 form a complex in which Filamin A connects MKK4 and MKK7γ2.

Filamin A enhances the activation of MKK7 and JNK

The above results suggested that Filamin A might be one of the 'binder' proteins predicted to closely connect two MAPKKs within a MAPK module in living cells [11]. To examine the effect of Filamin A on JNK activation *in vivo,* we compared JNK activation in M2 cells (no Filamin A expression) with that in A7 cells (M2 cells stably transfected with a vector expressing full-length human Filamin A; [16]). In response to increasing concentrations of sorbitol, JNK was activated much more strongly in A7 cells than in M2 cells (Figure 5A). When we analysed the activation state of MKK7 in these sorbitol-treated M2 and A7 cells, we found that 500 mM sorbitol induced a 3.3-fold activation of MKK7 in A7 cells, but only a 1.4-fold activation of MKK7 in M2 cells (Figure 5B). The activation of MKK4 is also higher in A7 cells than in M2 cells (Figure 5C). Thus, in living cells, Filamin A promotes optimal stress-induced JNK activation by enhancing MKK7 and MKK4 activation.

Finally, we analysed the effect of Filamin A on JNK activation induced by overexpression of MKK4 and/or MKK7γ2. M2 cells were transiently transfected with FLAG–MKK4 and FLAG–MKK7γ2, together with various amounts of FLAG–Filamin A. Overexpression of MKK7γ2 and MKK4 induced JNK activation which was greatly enhanced when the amount of transfected